Determination of the Polarization Observables C_x, C_z, and P_y for Final-State Interactions in the reaction $\vec{\gamma} d \rightarrow K^+ \vec{\Lambda} n$

Tongtong Cao

Advisor: Dr. Yordanka Ilieva

National Science Foundation
WHERE DISCOVERIES BEGIN

Jefferson Lab

Objective of This Work

To determine polarization observables C_x, C_z, and P_y for the final-state interactions in the reaction $\vec{\gamma} d \rightarrow K^+ \vec{\Lambda} n$.

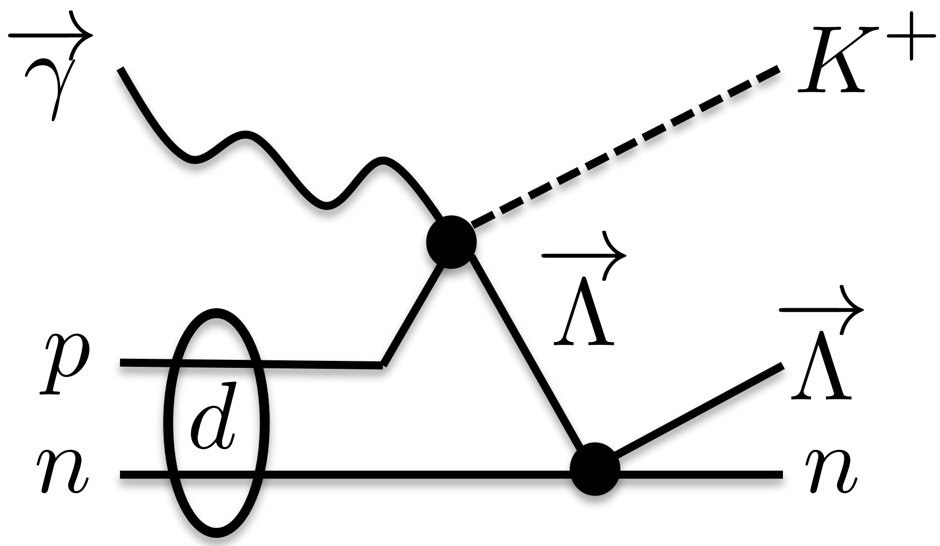

Step 1: $\vec{\gamma} p \rightarrow K^+ \vec{\Lambda}$

Step 2: $\vec{\Lambda} n \rightarrow \vec{\Lambda} n$

Study dynamics of Λn scattering

Outline

- Introduction: Why is the Λn dynamics important?
- Experimental Facility: Beam source and the detection system
- Data Analysis: Selection of the reaction and of yields
- Results: One-fold and two-fold differential estimates of the observables
- Discussion: What have we learned?
- Summary

Introduction

The Strong Interaction

The coupling constant in QCD, α_s, depends on the scale of the strong interaction.

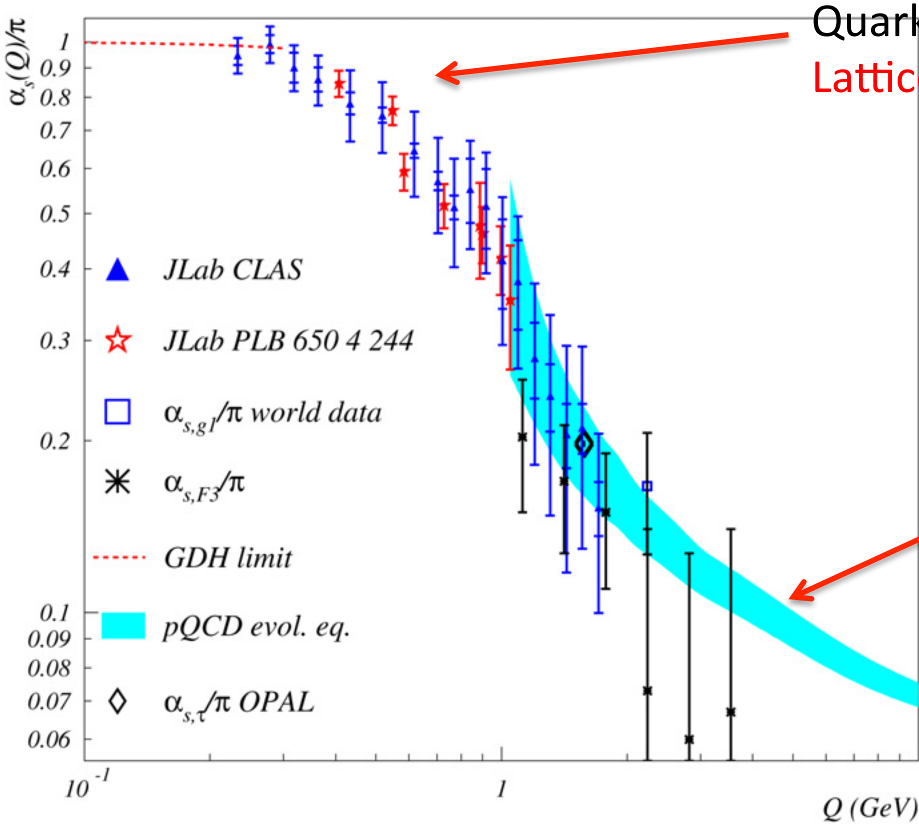

Quark confinement
Lattice QCD, Models

Asymptotic freedom
Perturbative QCD

Figure from: A. Deur et al., Physics Letters B 665, 349(2008).

The Baryon-Baryon Interaction

Examples of low–energy phenomena

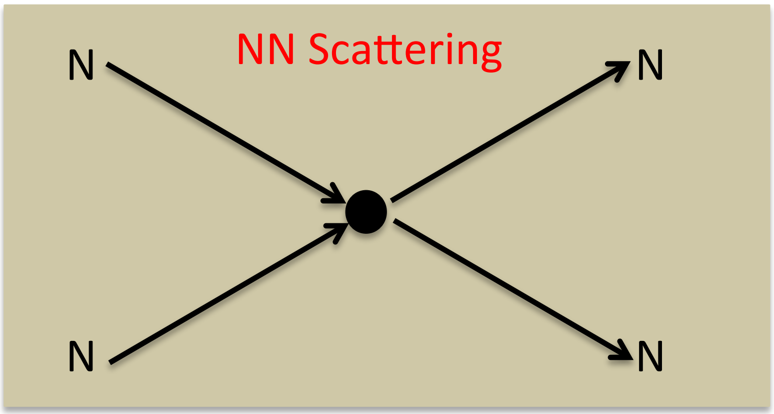

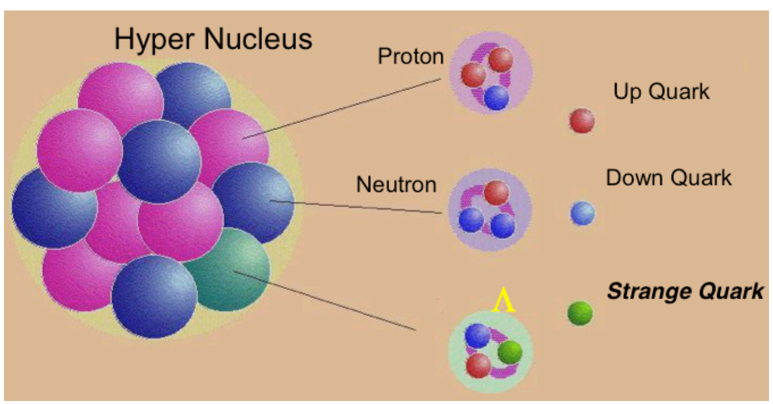

- Many low-energy phenomena can be described in terms of baryon-baryon interaction considering baryons to be elementary particles.

- Baryon-Baryon Interactions:
  - Nucleon-nucleon interaction
  - Hyperon-nucleon interaction
  - Hyperon-hyperon interaction

- If baryons are non-relativistic, baryon-baryon interactions can be described by potentials.

Bottom figure is from Satoshi N. Nakamura.

The Hyperon-Nucleon Interaction

The understanding of both hyperon-nucleon (YN) and nucleon-nucleon (NN) potentials is necessary to have a comprehensive picture of the strong interaction.

- Composition of dense nuclear matter (neutron stars interior).
- Many-body calculations of hypernuclei.

NN u d $\xrightarrow{\text{SU(3)}}$ YN u d s

Very well understood

SU(3) is broken → Some free parameters must be obtained from fits to YN experimental data

YN potential models: Meson-exchange models, Chiral effective field theory.

How to Constrain Hyperon-Nucleon Potentials

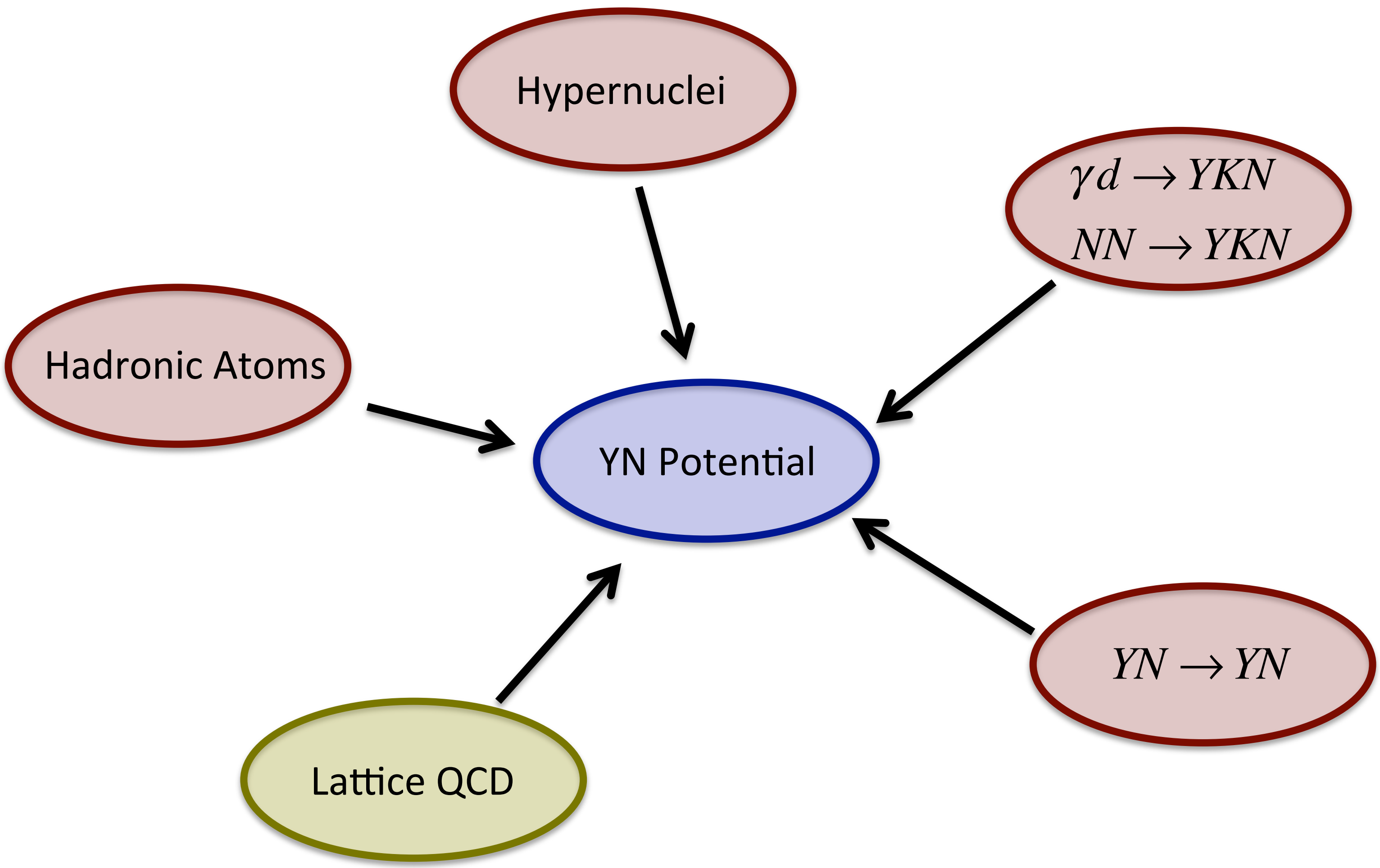

Dynamics of $\vec{\gamma} d \to K^+ \vec{\Lambda} n$

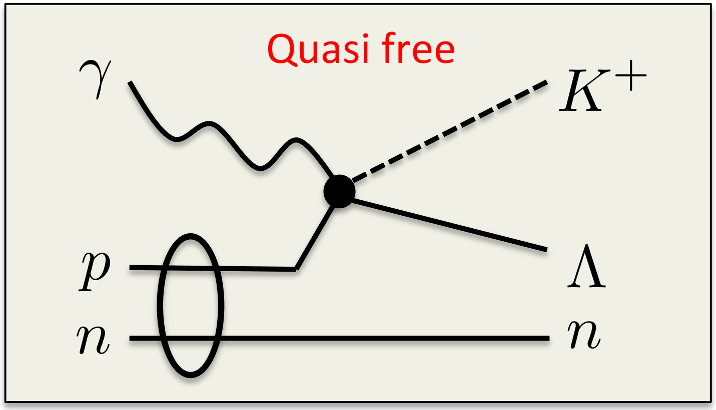

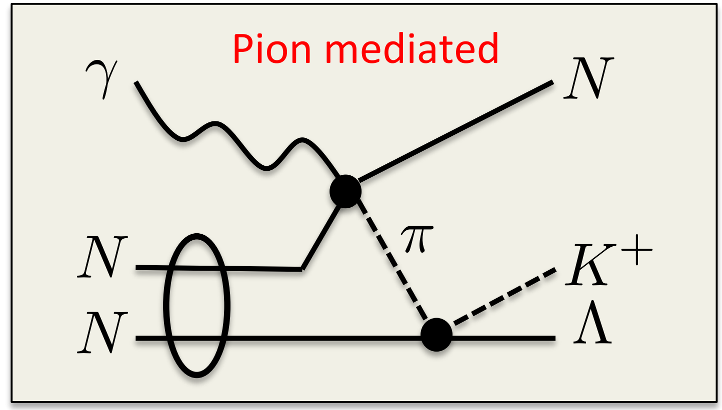

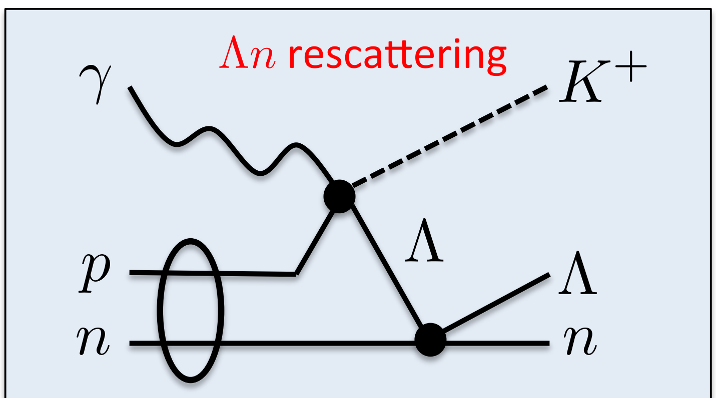

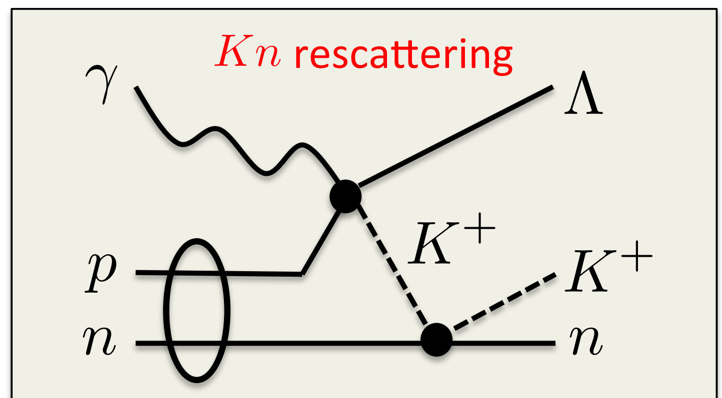

Λn elastic scattering ➔ constraints on YN potentials through model interpretation of observables.

Definition of Experimental Observables

General polarized differential cross section for hyperon photoproduction off the nucleon.

$$\frac{d\sigma^{\pm}}{d\Omega} = \frac{d\sigma}{d\Omega_0}(1 \pm \alpha P_{circ} C_x \cos\theta_x \pm \alpha P_{circ} C_z \cos\theta_z + \alpha P_y \cos\theta_y)$$

Λ self-analyzing power: α=0.642±0.013

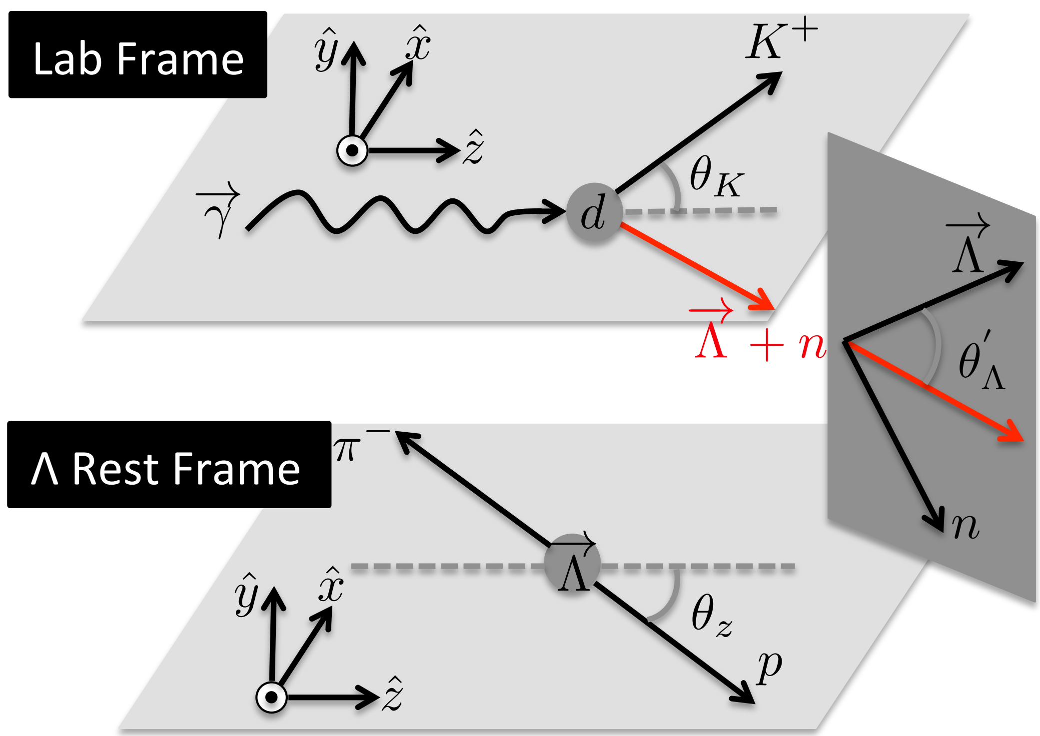

Theoretical Studies of $\vec{\gamma} d \to K^+ \vec{\Lambda} n$

- Calculations exist for single and double polarization observables as well as the cross section.
- Two YN potentials, Nijmegen NSC97f and NSC89, lead to very different predictions of polarization observables at some kinematics.
- Advantage: NSC97f and NSC89 both reproduce the binding energy of the hypertriton.
- Exclusive hyperon photoproduction off the deuteron can place unique constraints on YN potential parameters

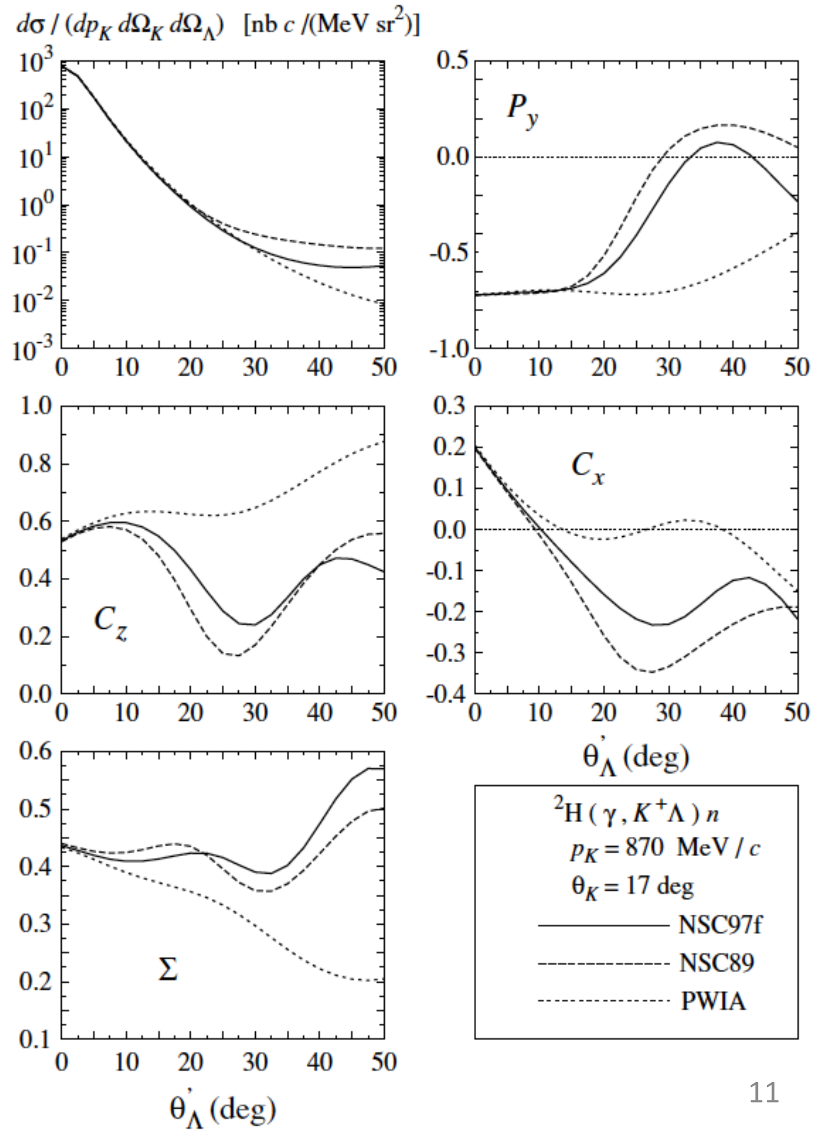

Figure from: K. Miyagawa et al., Phys. Rev. C 74, 034002 (2006).

Theoretical Studies of $\vec{\gamma} d \rightarrow K^+ \vec{\Lambda} n$

Dispersion Integral Method

- Allows to extract a spin-average YN scattering length from *Λn* invariant mass distributions.

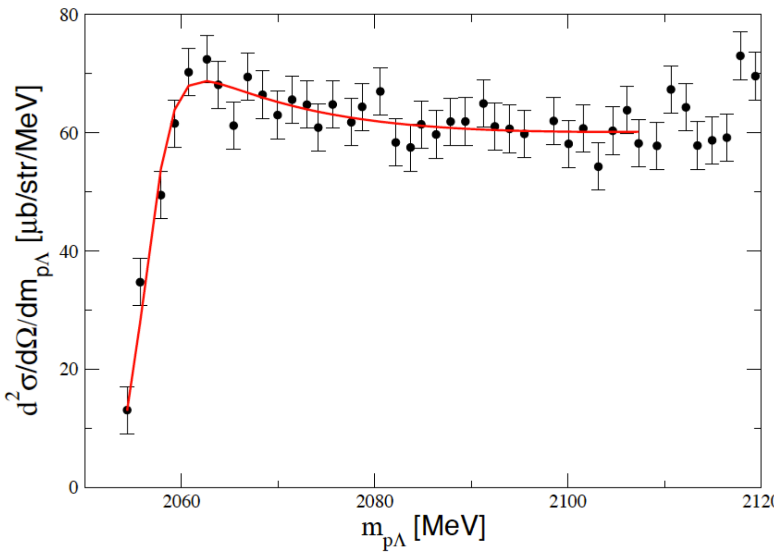

- Applied to cross section data of

$$pp \rightarrow K^+ X$$

Spin-average *Λp* scattering length:

a = -1.5 ± 0.15 ± 0.3 fm

- Similar uncertainties expected for analysis of photoproduction data.

- *Λp* scattering length by ESC-model:

a_{1s0} = - 2.20 ± 1.10 fm; a_{3s1} = - 1.75 ± 0.10 fm

Figure from: A. Gasparyan et al., Phys. Rev. C 69, 034006(2004).

Experimental Facility

The Continuous Electron Beam Accelerator Facility (CEBAF)

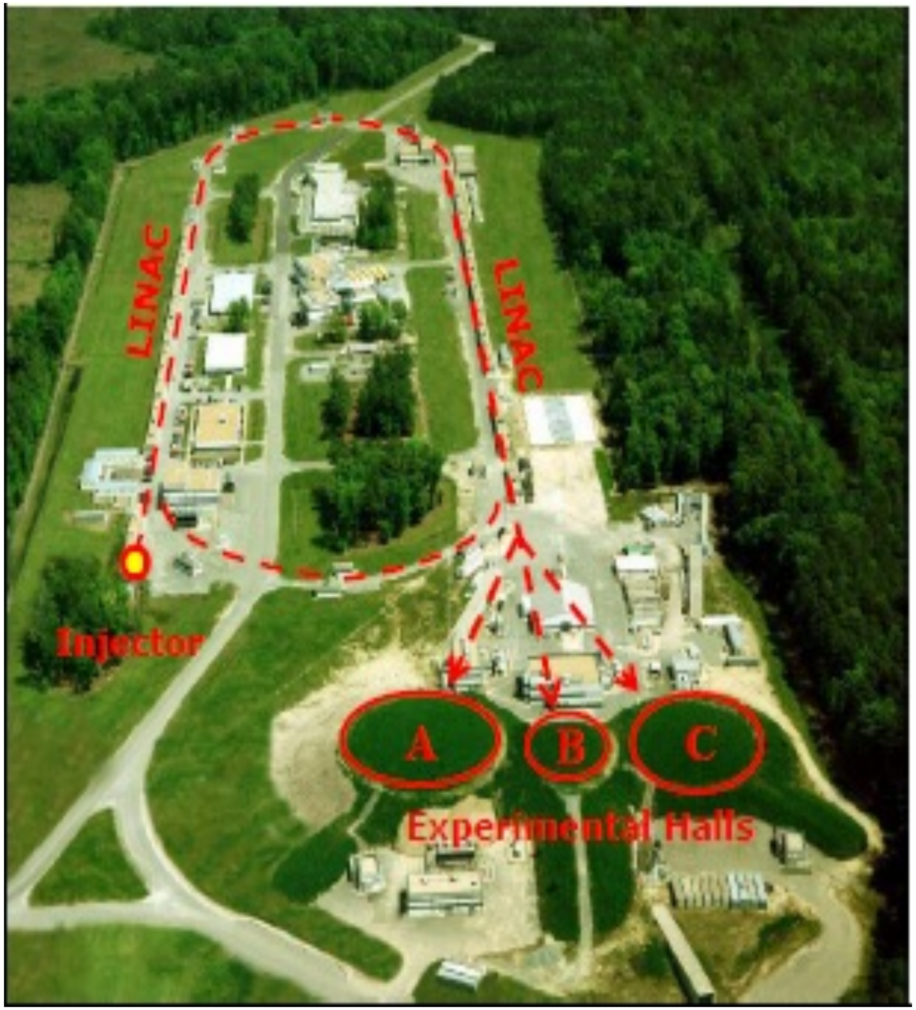

- Simultaneously provides electron beams to halls A, B, and C
- Polarization: Up to 85%
- Energy: Up to 6 GeV
- Currently: 12 GeV upgrade has been completed and a new hall D is in service

The Hall-B Photon Tagger

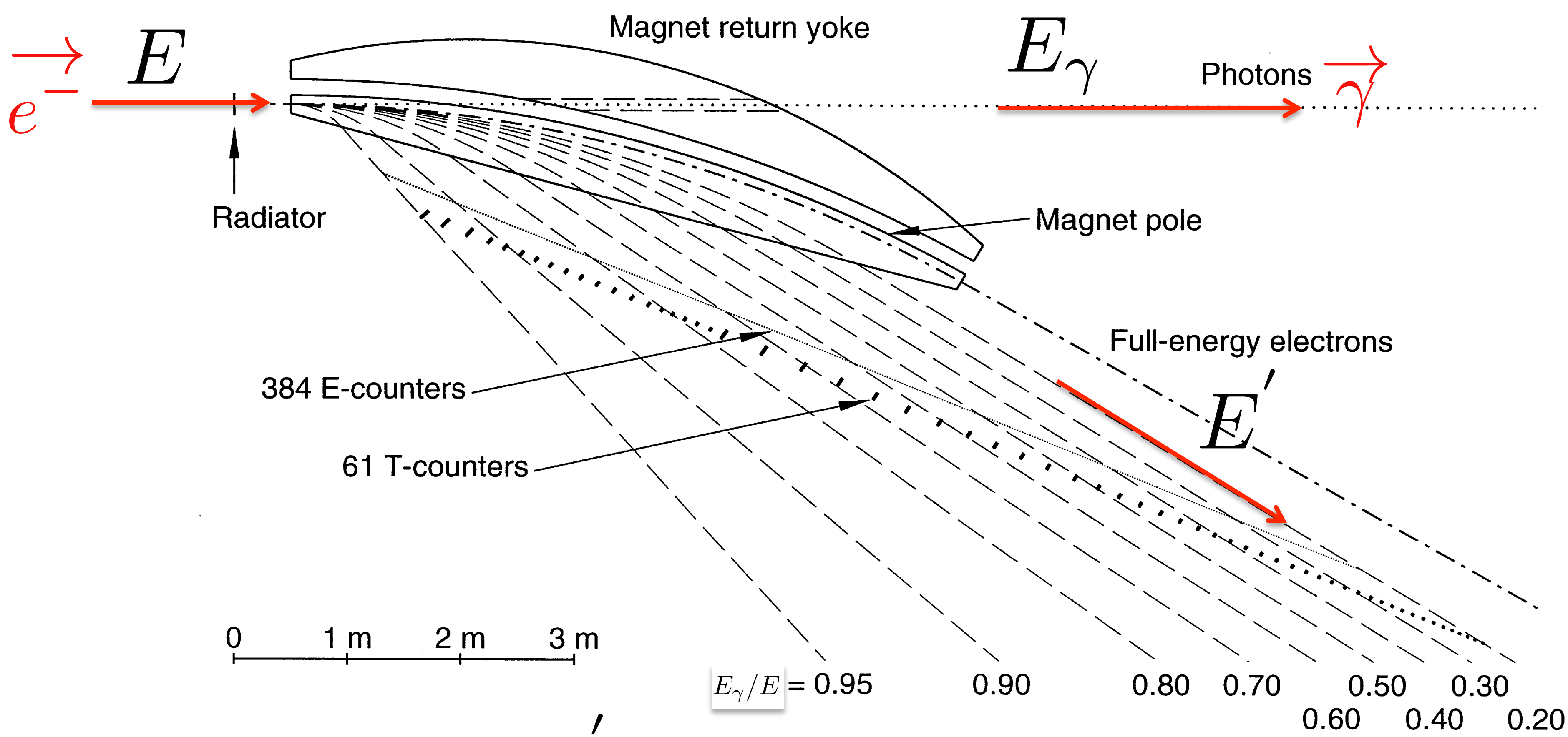

$$E_\gamma = E - E'$$

Energy resolution (GeV): $0.001 \times E$

Time resolution: 110 ps

Figure from: D. I. Sober et al., Nucl. Instr. Meth. A 440, 263(2000).

The CEBAF Large Acceptance Spectrometer (CLAS)

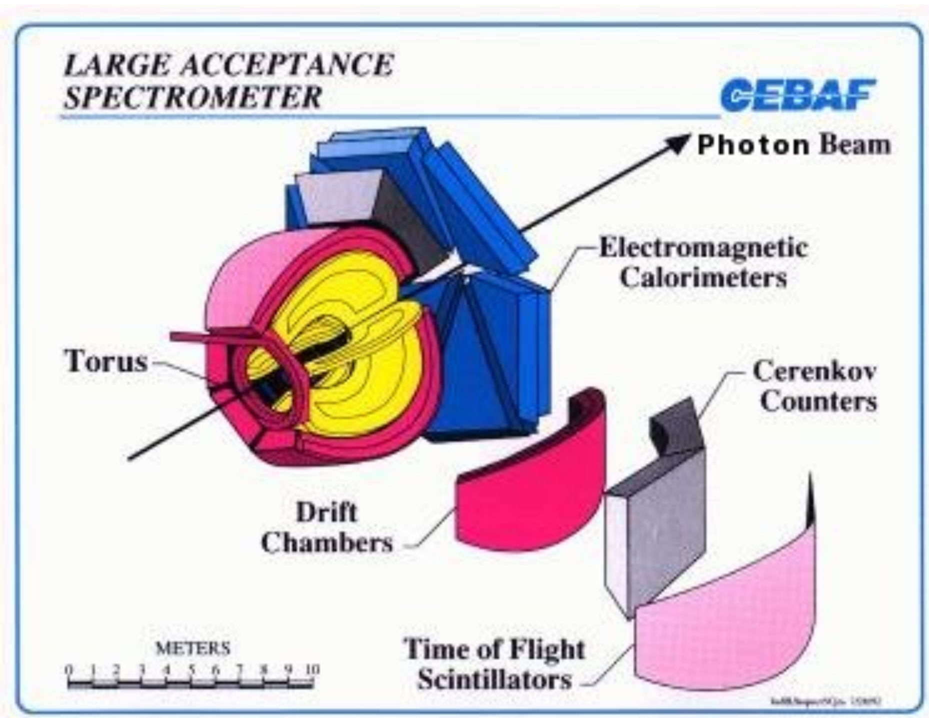

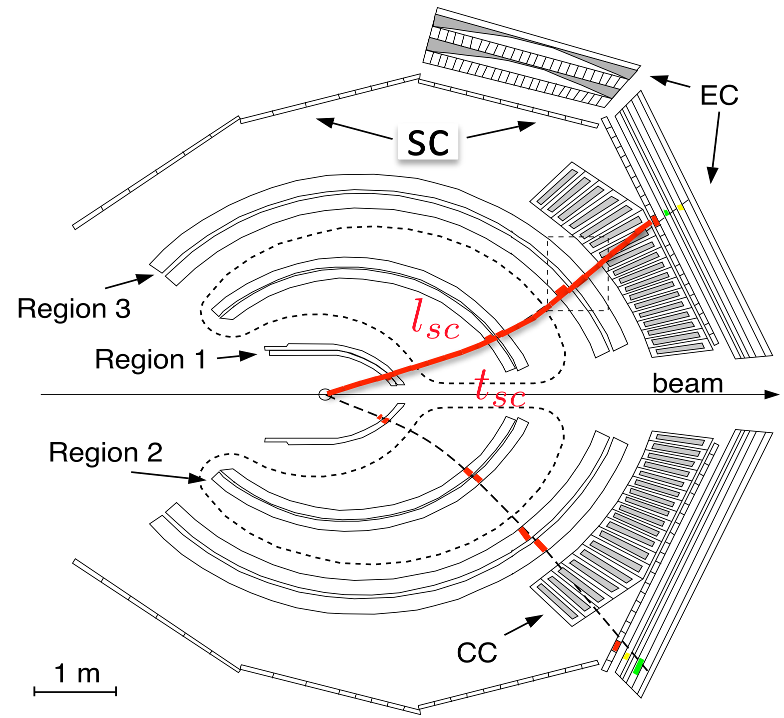

Speed of a Particle: $\beta_{meas} = \dfrac{l_{sc}}{ct_{sc}}$

Figure from: B. Mecking et al. Nucl. Instr. Meth. A 503, 513(2003).

The E06-103 Experiment (g13)

- Circularly polarized photon beam (g13a)
- E_e = 1.987 GeV; 2.649 GeV
- Electron beam polarization: [77%, 85%]
- Photon beam polarization: [27%, 80%]
- Target: LD_2, unpolarized, 40-cm long

$$\vec{\gamma}\, d \rightarrow \boxed{K^+}\, \vec{\Lambda}\, n$$

$$\vec{\Lambda} \rightarrow \boxed{p\pi^-}$$

Detected in CLAS

Data Analysis

Particle Identification (PID)

- Events with two positively-charged and one negatively-charged particles were selected for analysis of $\vec{\gamma} d \to K^+ \vec{\Lambda} n$.

- PID control variable

$$\Delta\beta = \beta_{meas} - \beta_{calc} = \beta_{meas} - \sqrt{\frac{p^2}{m^2 + p^2}}$$

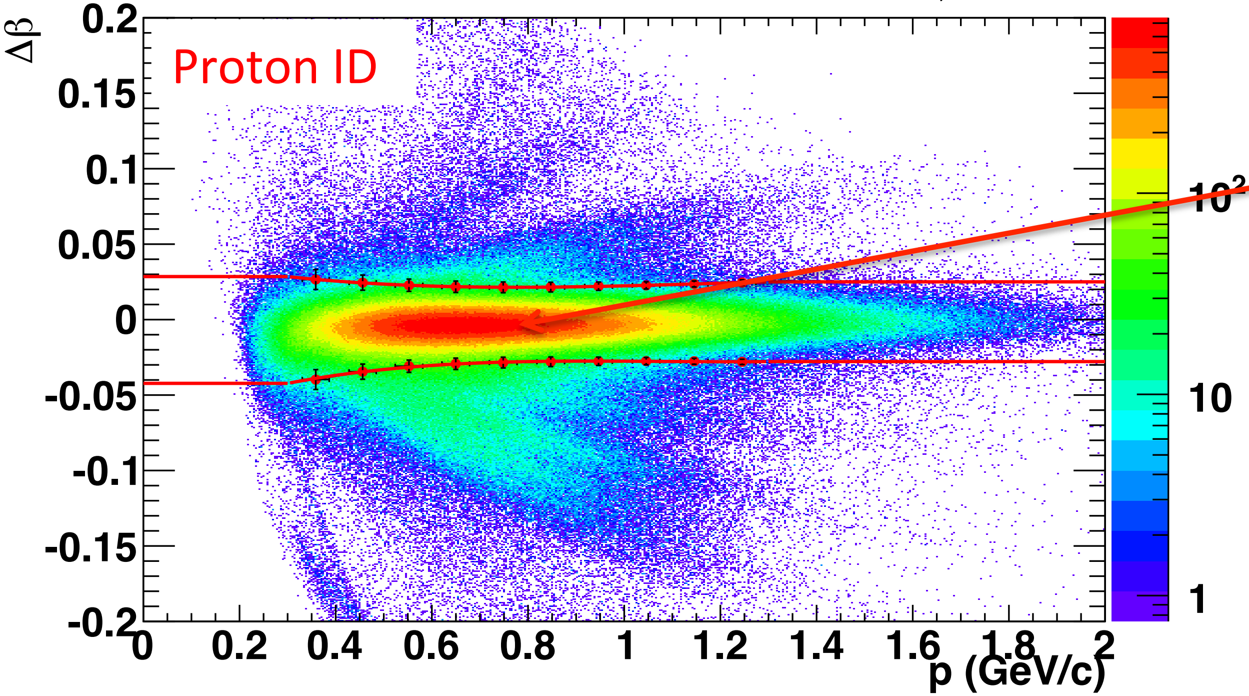

p: [0.7, 0.8] GeV/c

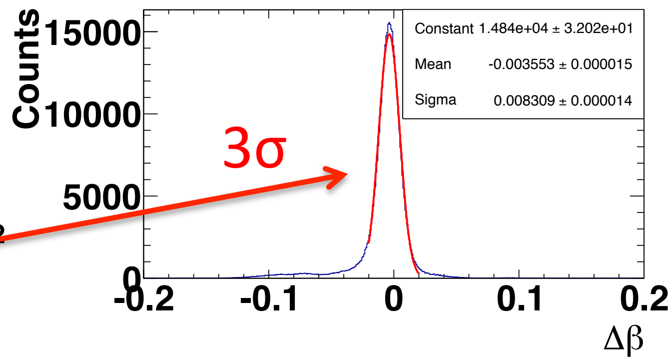

Photon Selection

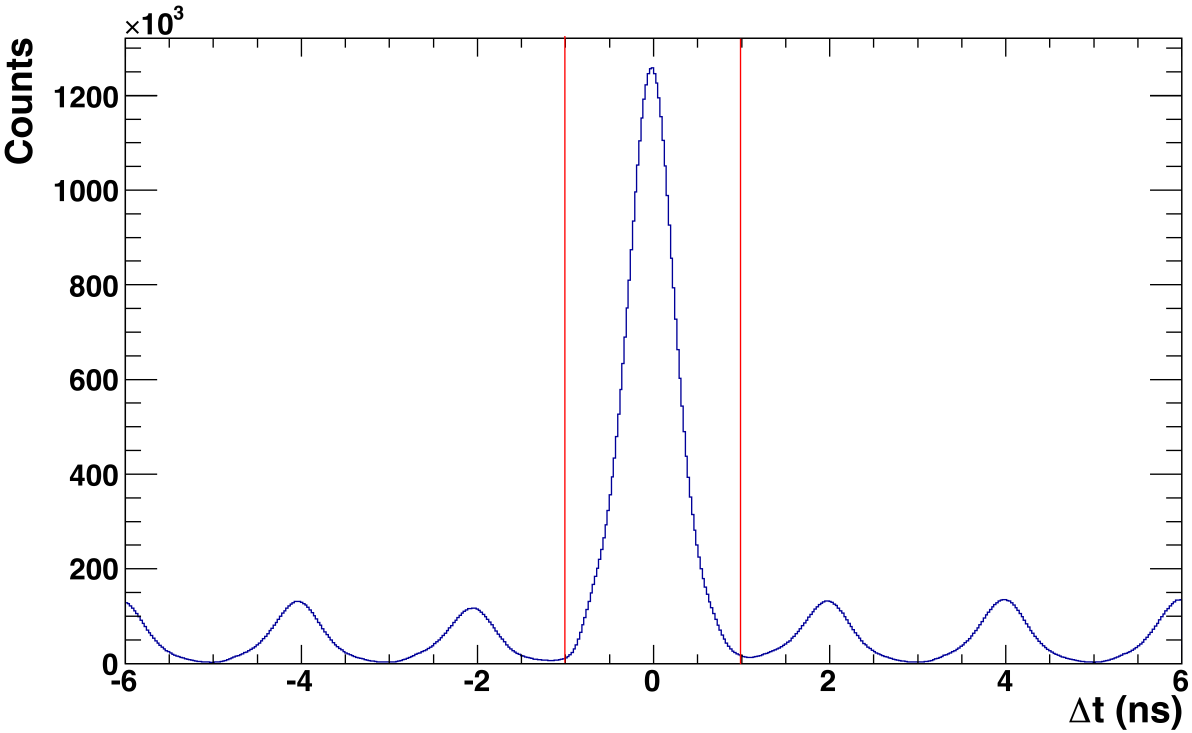

Electron beam delivered as bunches every 2.004 ns from CEBAF.

High beam current, wide tagger TDC readout window.

On average 14 photons were recorded for each event.

$$\Delta t = t_v - t_\gamma = (t_{sc} - \frac{l_{sc}}{c\beta_{calc}}) - (t_{TAGR} + \frac{z + 20(cm)}{c})$$

Extraction of Final-State Interaction Events

$$IM \equiv M_{p\pi^-} = \sqrt{(\widetilde{p}_p + \widetilde{p}_\pi)^2}$$

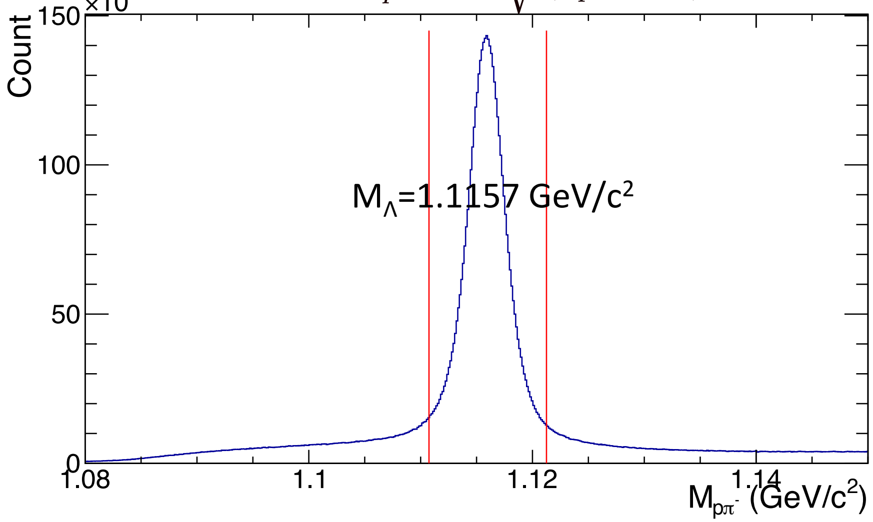

$$MP \equiv P_X \ (\vec{\gamma} d \to K^+ \vec{\Lambda} X)$$

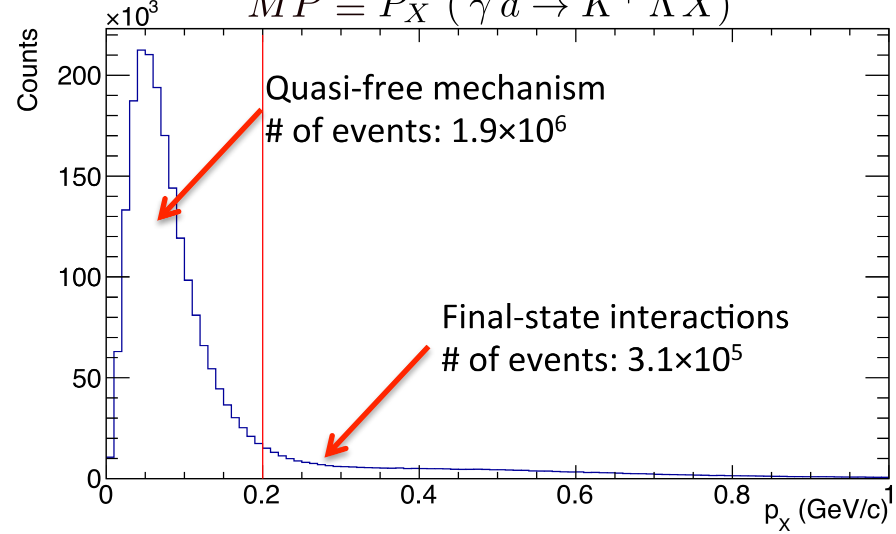

$$MM \equiv M_X = \sqrt{(\widetilde{p}_\gamma + \widetilde{p}_d - \widetilde{p}_{K^+} - \widetilde{p}_p - \widetilde{p}_{\pi^-})^2}$$

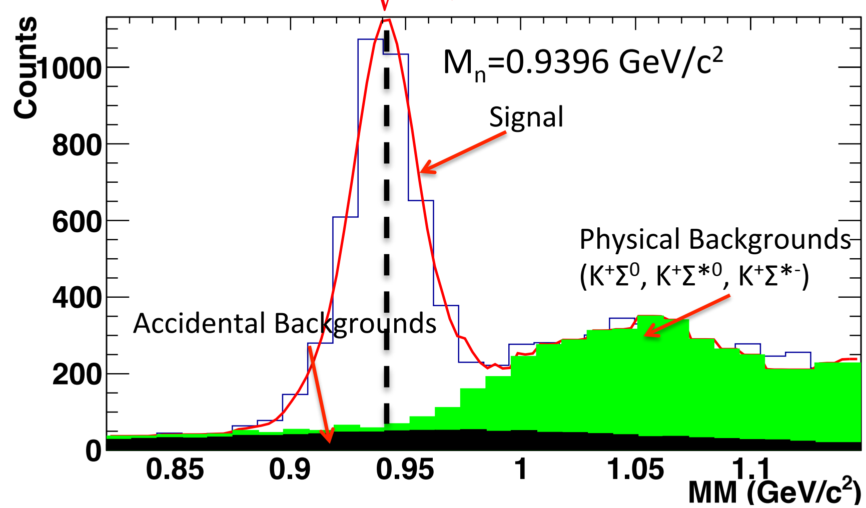

Results

Observable-Extraction Method

The maximum likelihood method was used to extract the observables.

Probability density function defined from the polarized differential cross section:

$$L_i = \frac{d\sigma}{d\Omega_0}(1 \pm \alpha P^i_{circ} C_x \cos\theta^i_x \pm \alpha P^i_{circ} C_z \cos\theta^i_z + \alpha P_y \cos\theta^i_y)$$

Total likelihood is the product of the likelihoods for all individual events:

$$logL = b + \sum_{i=1}^{n^+} log[(1 + \alpha P^i_{circ} C_x \cos\theta^i_x + \alpha P^i_{circ} C_z \cos\theta^i_z + \alpha P_y \cos\theta^i_y) w^i]$$

$$+ \sum_{j=1}^{n^-} log[(1 - \alpha P^j_{circ} C_x \cos\theta^j_x - \alpha P^j_{circ} C_z \cos\theta^j_z + \alpha P_y \cos\theta^j_y) w^j]$$

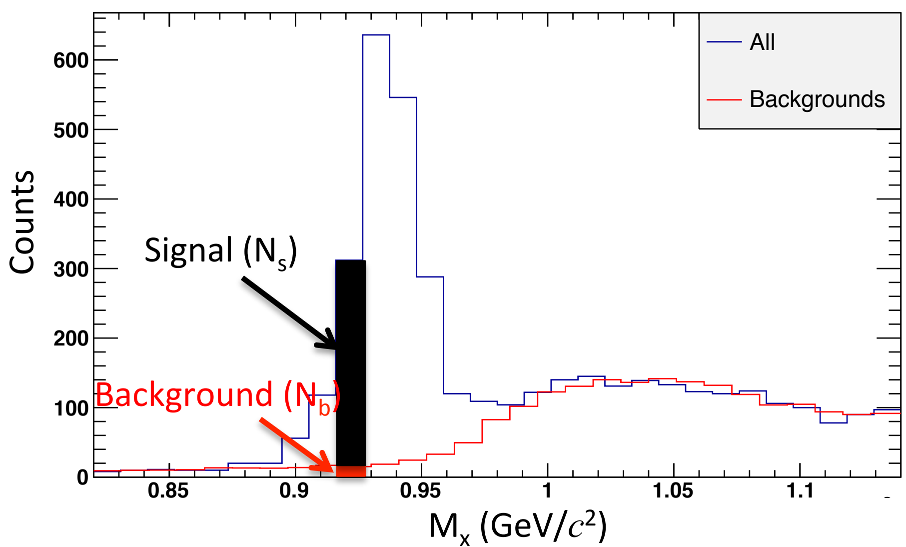

$$w^i \text{ or } w^j = \frac{N_s}{N_s + N_b}$$

Axis Convention

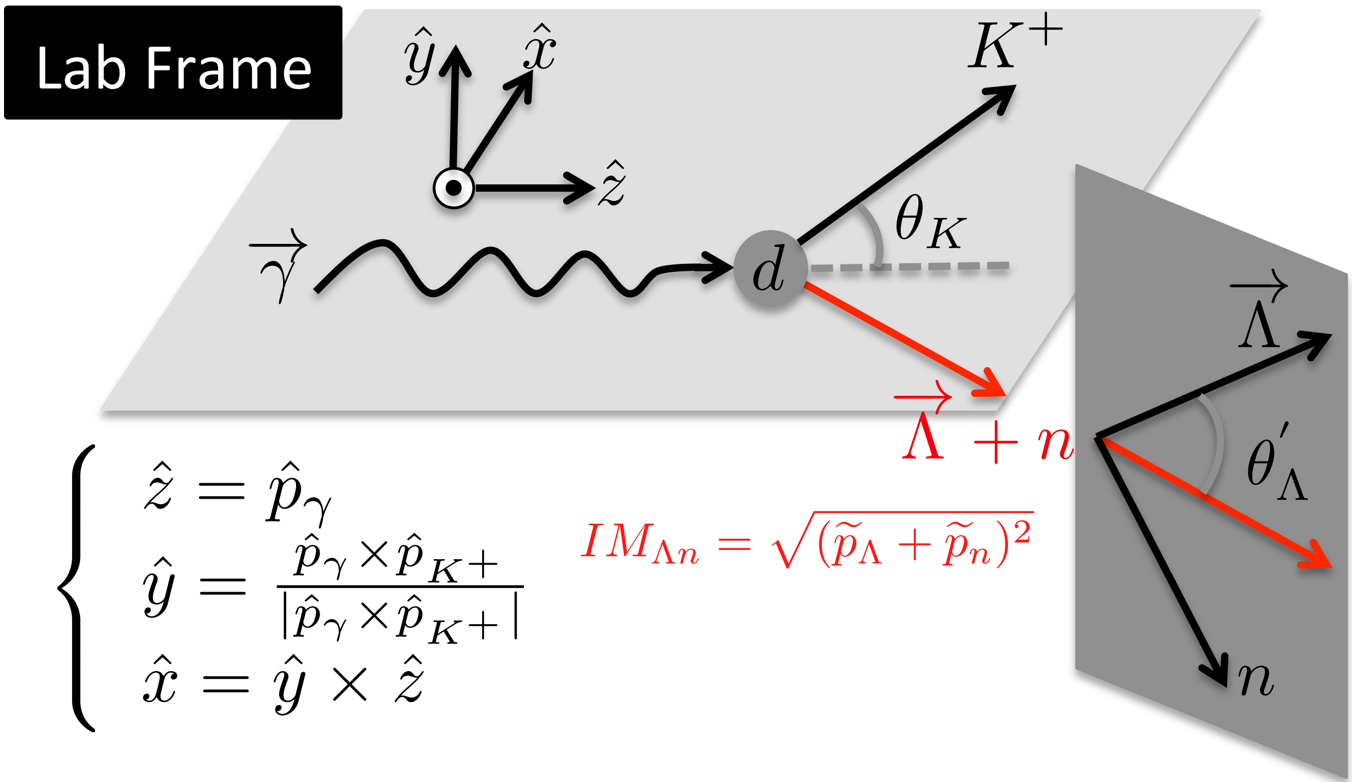

$$
\begin{cases}
\hat{z} = \hat{p}_\gamma \\
\hat{y} = \dfrac{\hat{p}_\gamma \times \hat{p}_{K^+}}{|\hat{p}_\gamma \times \hat{p}_{K^+}|} \\
\hat{x} = \hat{y} \times \hat{z}
\end{cases}
$$

$$IM_{\Lambda n} = \sqrt{(\widetilde{p}_\Lambda + \widetilde{p}_n)^2}$$

Data are binned in E_γ, θ'_Λ, p_K, θ_K, and $IM_{\Lambda n}$.

One-fold Differential Estimates
Bin Setup

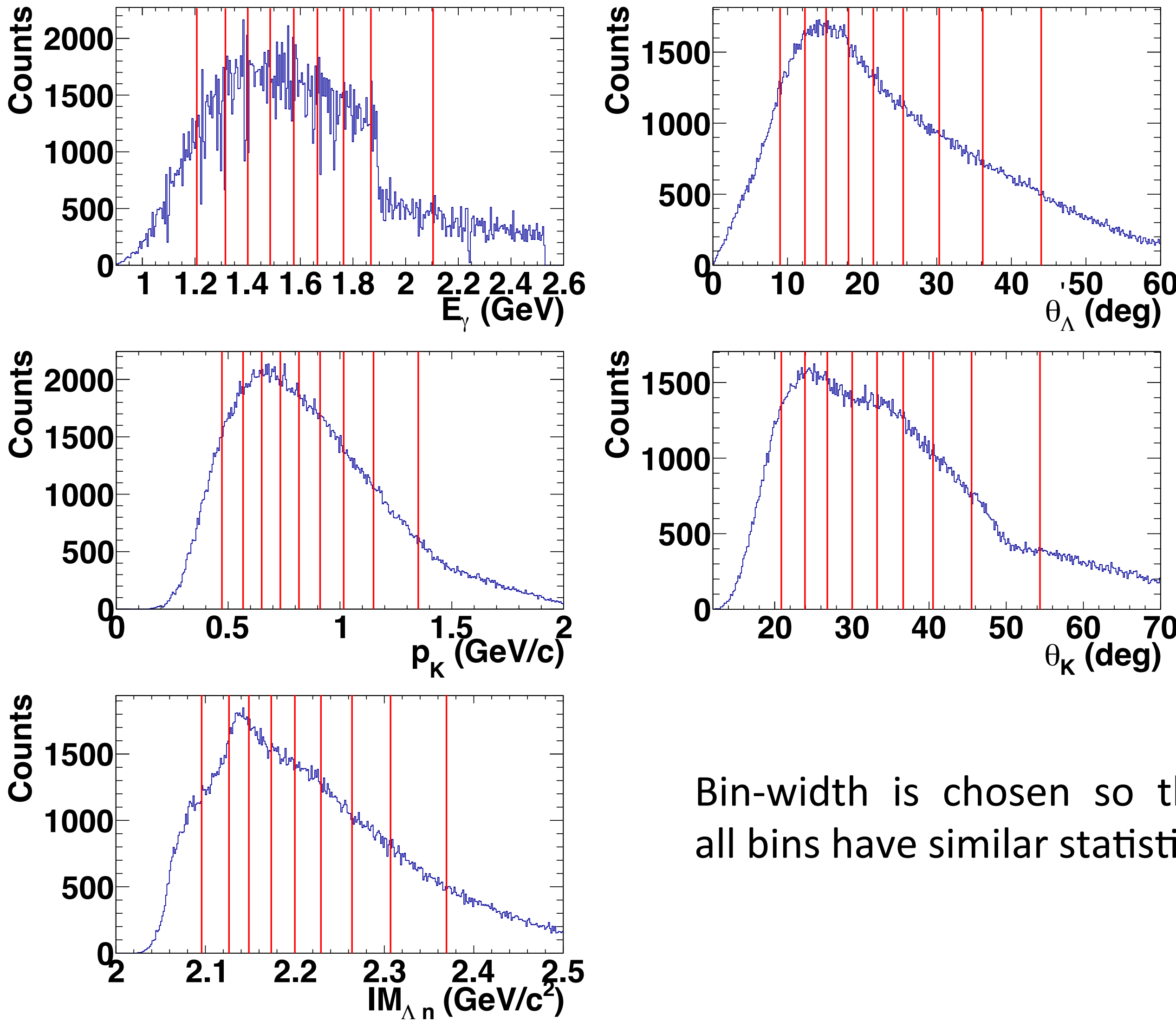

Bin-width is chosen so that all bins have similar statistics.

One-fold Differential Estimates

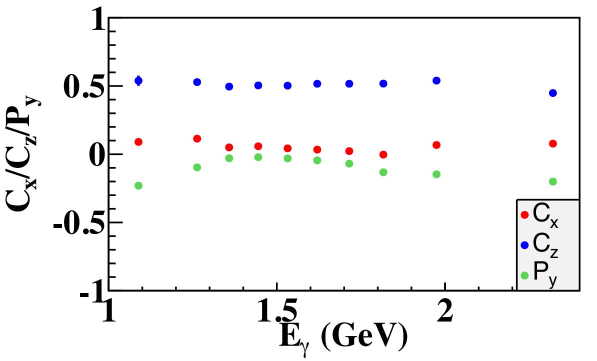

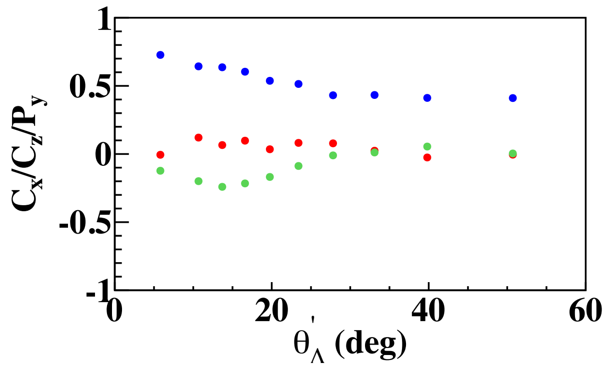

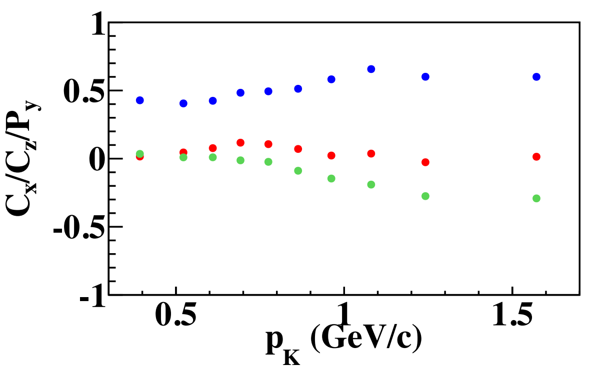

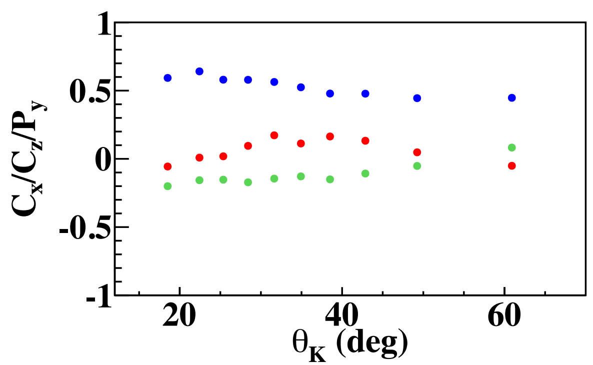

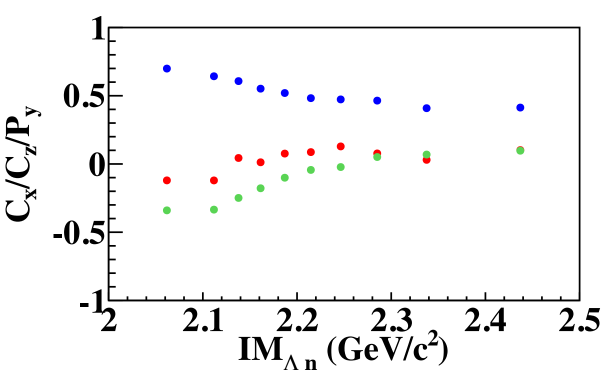

- Overall, C_x is small and varies around 0, Cz varies between 0.4 and 0.8, and Py varies between -0.4 and 0.1.
- The observables have a weaker dependence on E_γ than on other kinematics variables.

Statistical uncertainties:

- C_x: [0.020, 0.045]
- Cz: [0.024, 0.051]
- Py: [0.016, 0.029]

Two-fold differential estimates
Bin Setup in $IM_{\Lambda n}$ and θ'_{Λ}

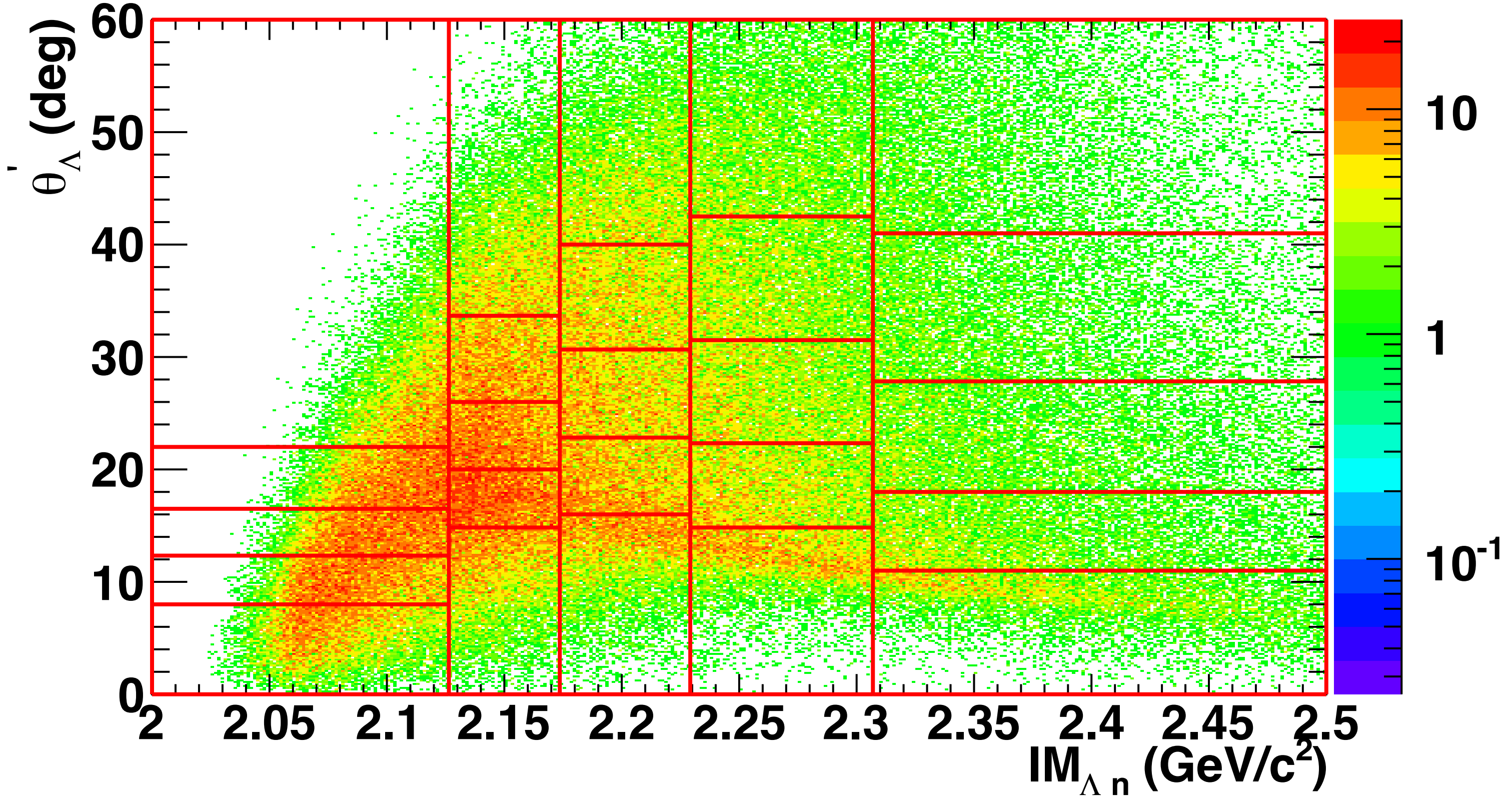

Two-fold differential estimates $C_x(IM_{\Lambda n}, \theta'_\Lambda)$, $C_z(IM_{\Lambda n}, \theta'_\Lambda)$, and $P_y(IM_{\Lambda n}, \theta'_\Lambda)$

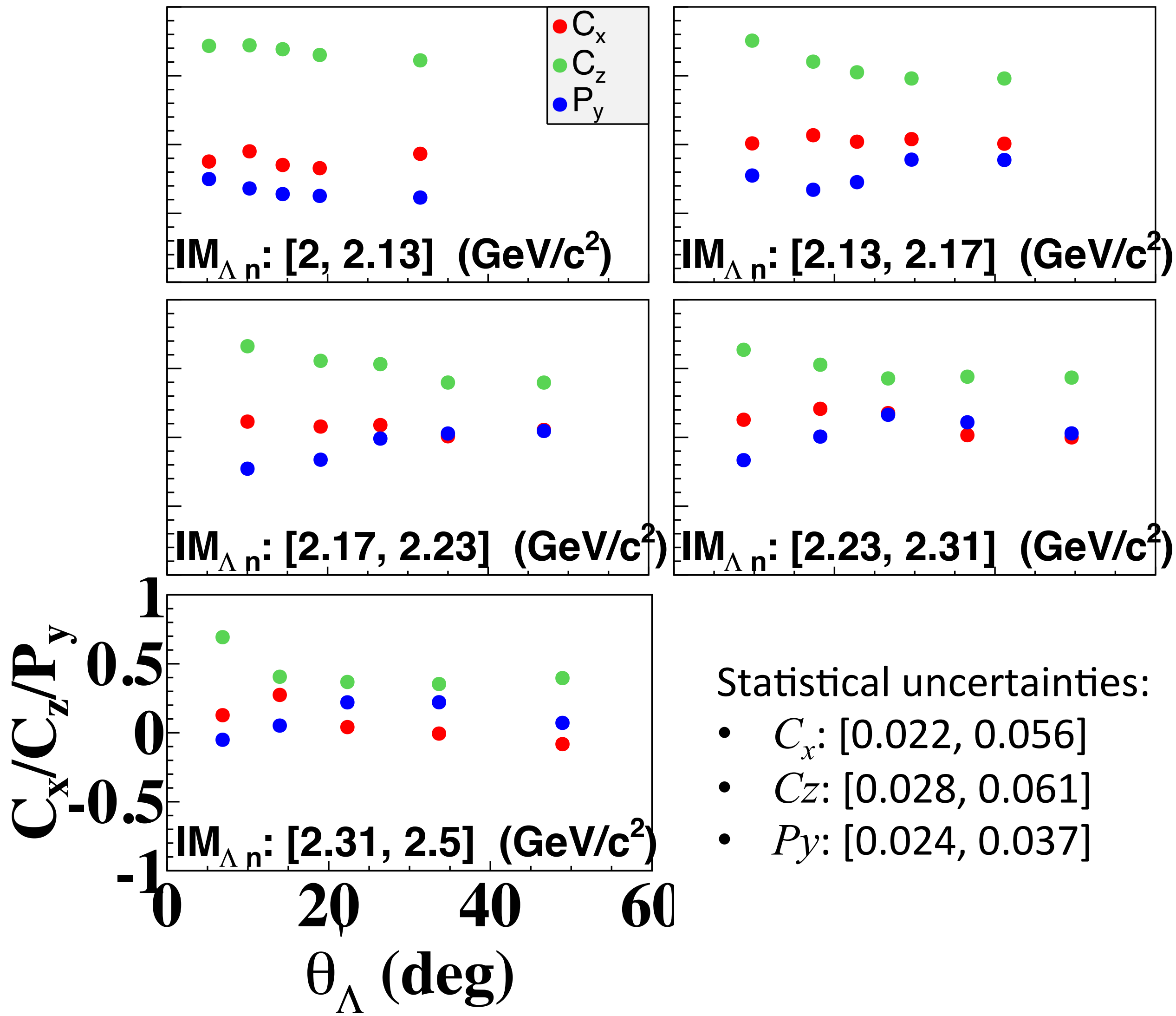

Statistical uncertainties:

- C_x: [0.022, 0.056]
- Cz: [0.028, 0.061]
- Py: [0.024, 0.037]

- C_x is small and varies around 0.
- Overall, Cz decreases as θ'_Λ increases.
- Py shows different variation tendency as θ'_Λ increases for different $IM_{\Lambda n}$ bins.

Systematic Uncertainties

Source	C_x	C_z	P_y
CLAS Acceptance	5.5%	0.3%	3.5%
Fiducial Cut	0.1%	0.3%	0.1%
Photon Polarization	4.1%	4.1%	0%
PID	2.7%	2.7.%	0.2%
Vertex Cut	1.4%	0%	0.1%
Photon Selection	0.1%	0.3%	0.1%
IM Cut	1.4%	0.7%	0.3%
MP Cut	0.6%	0.2%	0.1%
MM Cut	1.6%	3.2%	2.1%
Λ Self-analyzing Power	2.0%	2.0%	2.0%
Total	8.1%	6.2%	4.6%

Discussion

Discussion: Comparison to CLAS g1c Results

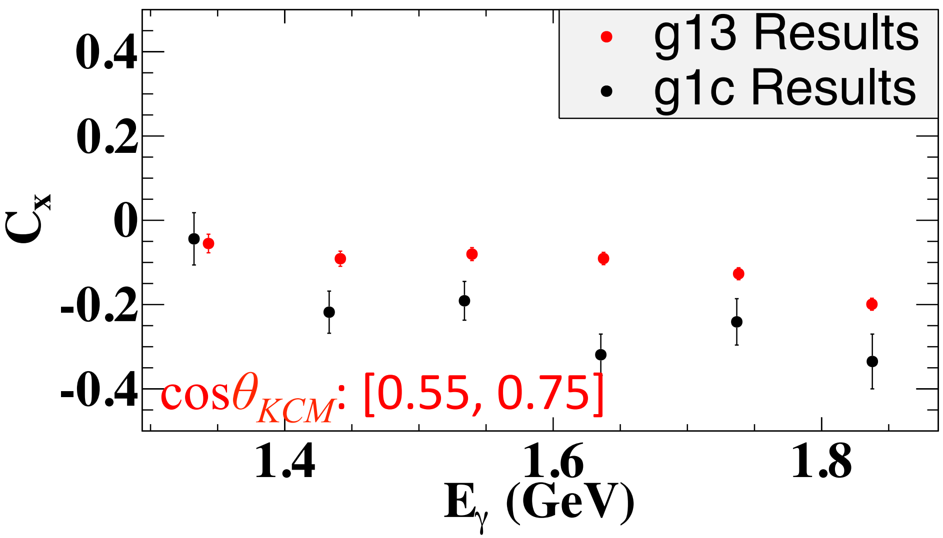

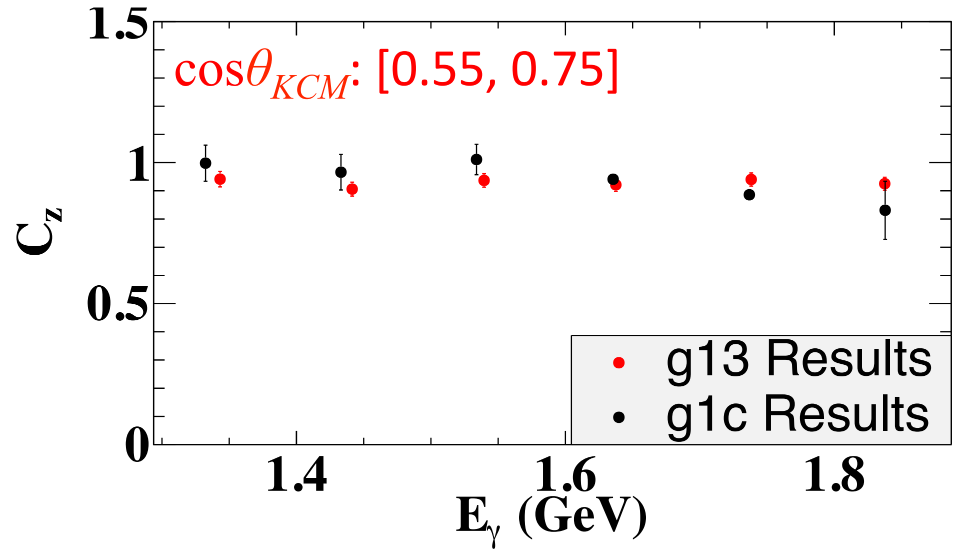

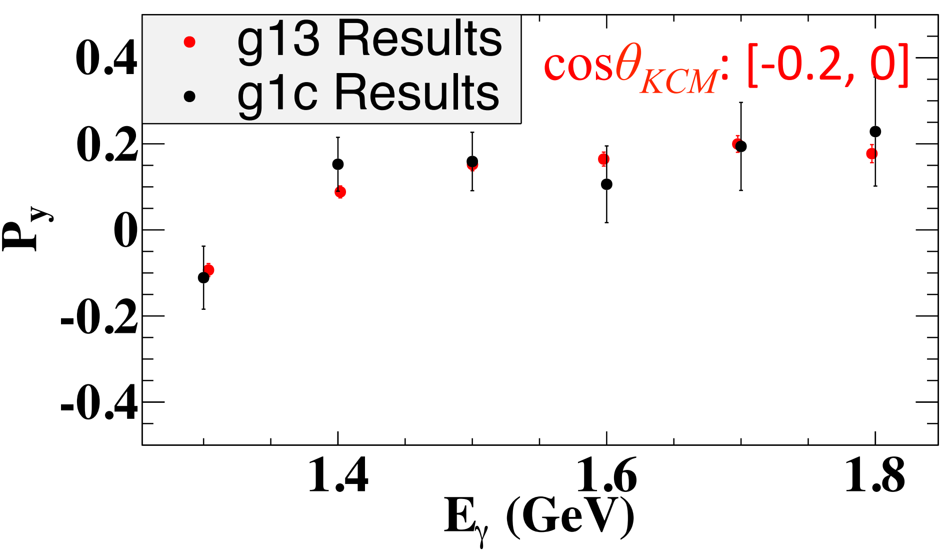

C_x and C_z from Robert K. Bradford and P_y from John W.C. McNabb

- Dataset: CLAS g1c
- Reaction: $\overrightarrow{\gamma} p \to K^+ \overrightarrow{\Lambda}$

Comparison Between QF and FSI

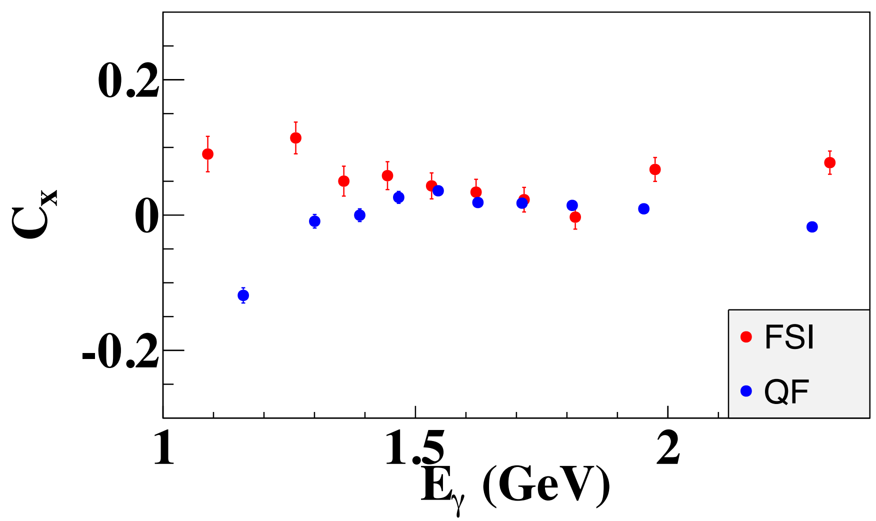

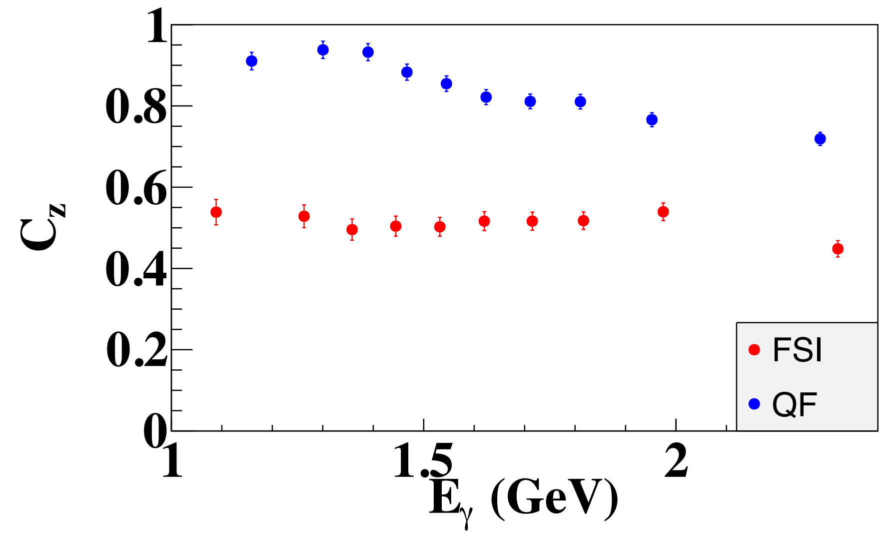

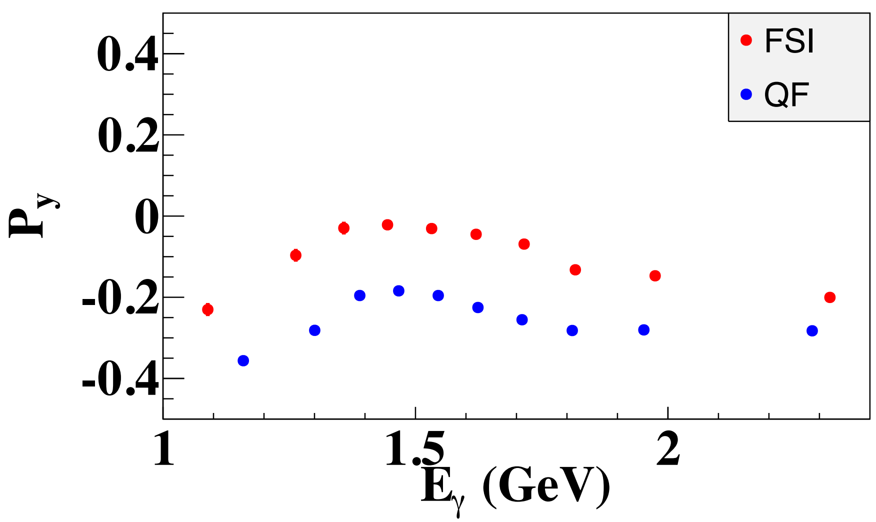

- Cx: At lower photon energy, there is a big difference between QF and FSI. At higher photon energy, the differences are small.
- Cz: QF values are close to 1, and are systematically larger than FSI.
- Py: FSI values are larger than QF values for all E_γ.

Effect of Missing Momentum Cut

$\cos\theta_{KCM}$: [0.15, 0.35]

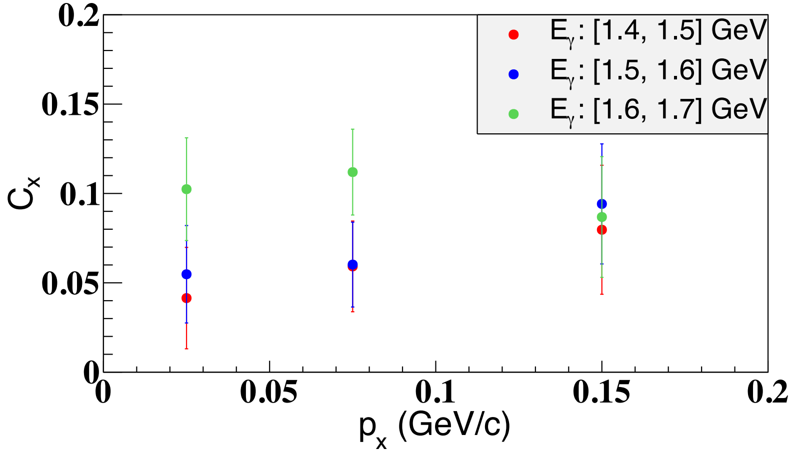

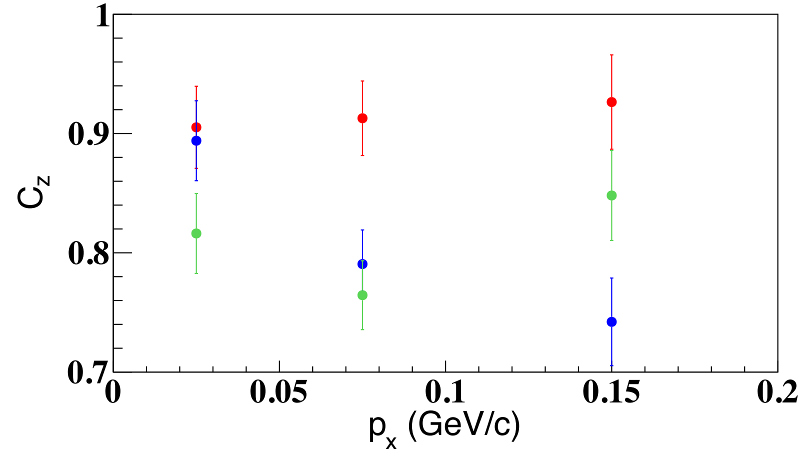

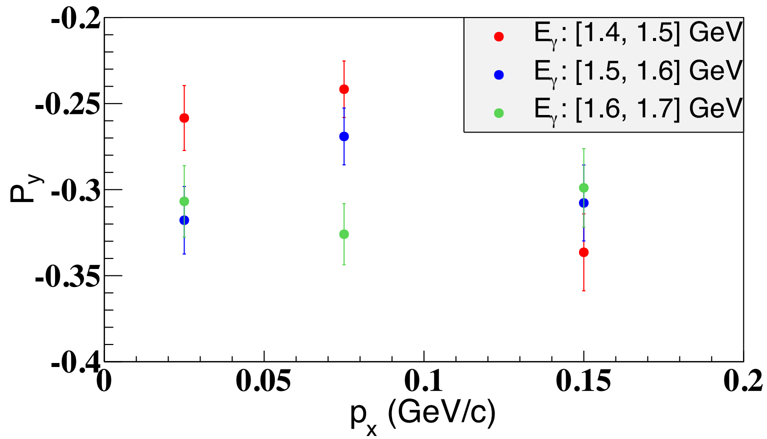

The missing momentum is cut within different ranges are not overlapping: 0 – 0.05 GeV/c, 0.05 – 0.1 GeV/c, and 0.1 – 0.2 GeV/c.

Effect of the Quasi-free Mechanism

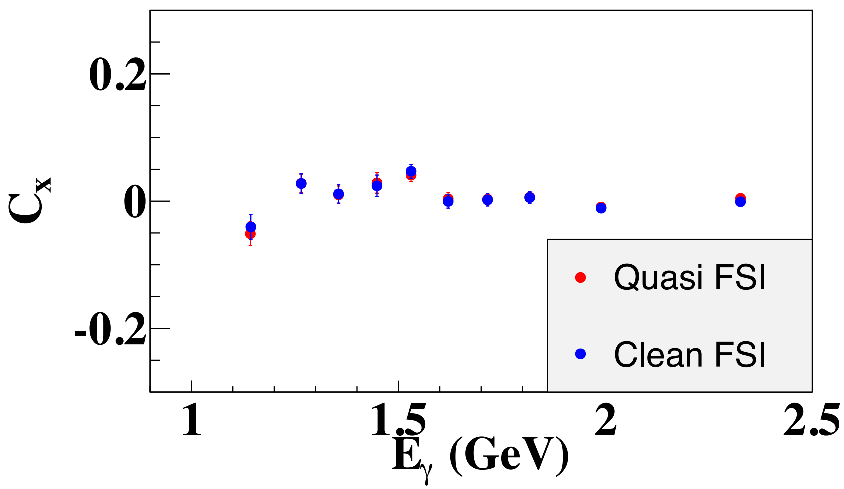

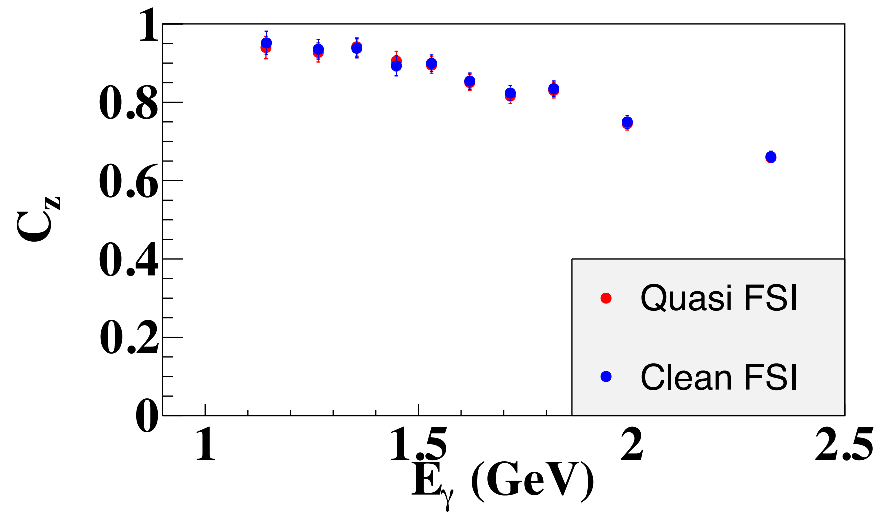

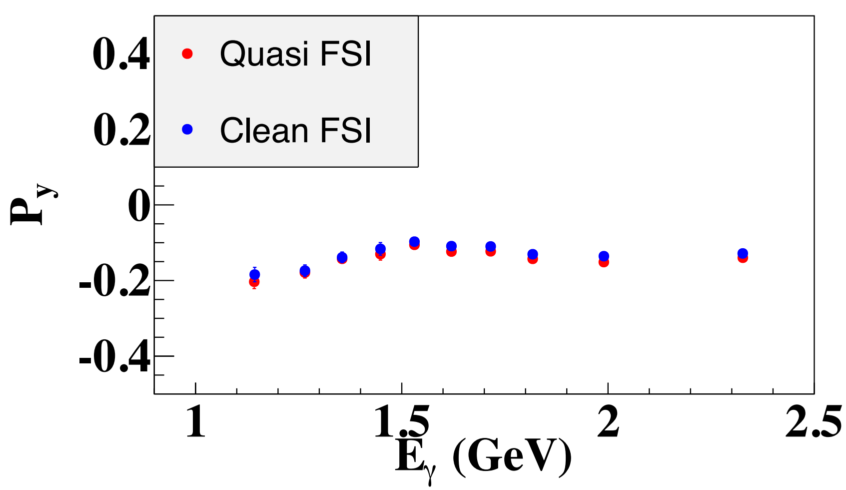

- Observables are extracted from two simulated samples:
  - Sample 1: Clean final-state-interaction events
  - Sample 2: Sample 1 plus a small sample of quasi-free events
- Sample 2 is smeared with 12% of the quasi-free mechanism

Theoretical Predictions and Data

K. Miyagawa et al., Phys. Rev. C 74, 034002 (2006).

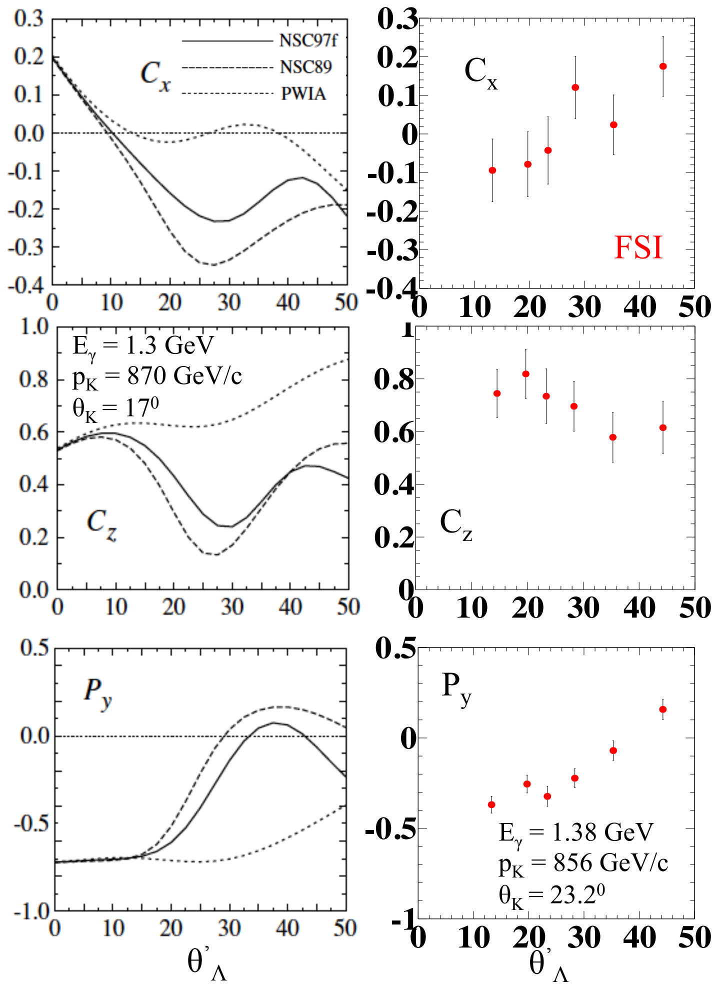

E_γ = 1.3 GeV,
p_K = 900 MeV/c,
θ_K = 17 deg

- Due to limited statistics, in a small range of kinematics, the background subtraction method is not applicable, and yields are extracted by means of a missing-mass cut.
- Four-fold differential estimates can be obtained with reasonable statistical uncertainties.
- Qualitative comparison of general features only
  - Data: FSI, Model: QF+FSI
  - $\theta_{K,Data} > \theta_{K,Model}$

Range: $E_{\gamma:}$ [1.1, 1.5] GeV, $p_{K:}$ [700, 1150] MeV/c, $\theta_{K:}$ [14, 27] deg
Average: E_γ = 1.38 GeV, p_K = 856 MeV/c, θ_K = 23.2 deg

Data for Λn Scattering Length Determination

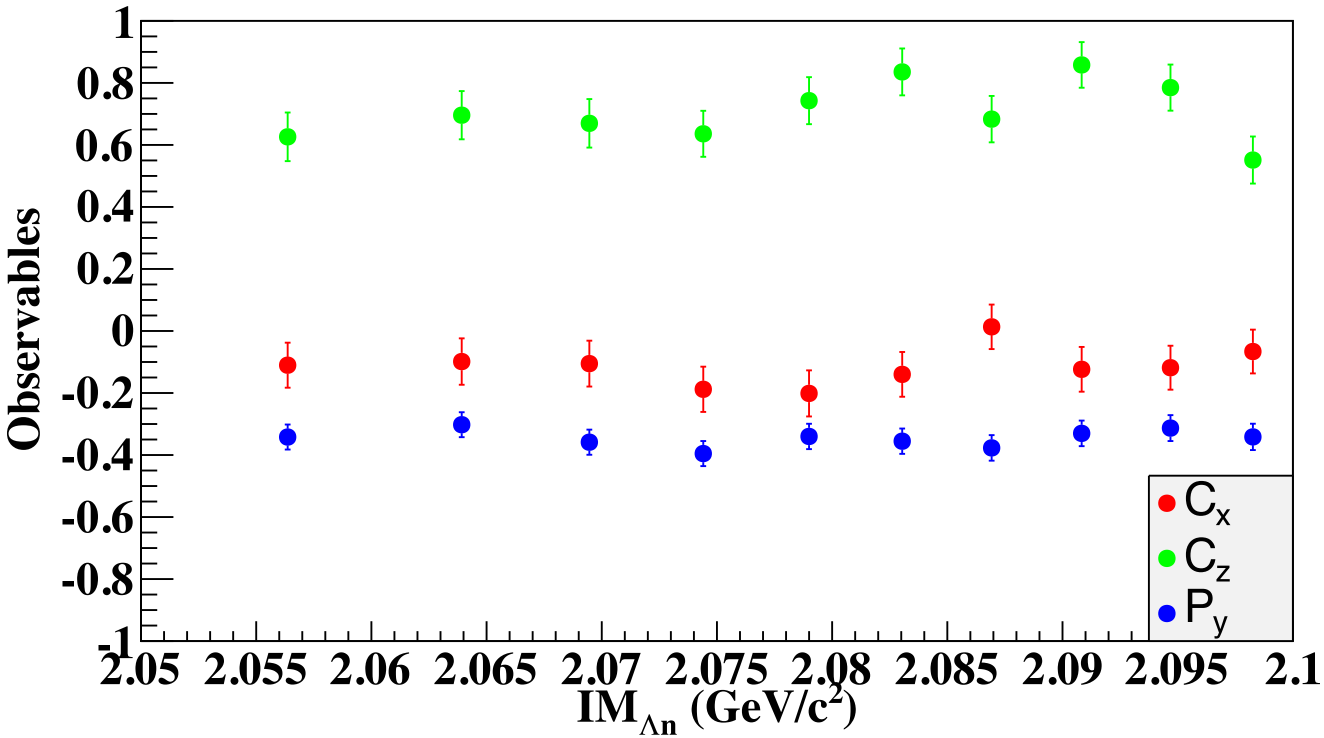

Offer an opportunity to extract a spin-average Λn scattering length using Gasparyan's method.

Contribution of QF in FSI Sample

Cut (GeV/c)	δ	f	p_{FSI}^{lost}
0.20	1.27%	31.39%	10.19%
0.25	1.86%	18.78%	15.09%
0.30	2.53%	11.83%	20.85%
0.35	3.26%	7.85%	27.44%
0.40	4.04%	4.94%	32.69%

δ : FSI contribution for data sample with missing momentum less than cut point.

f : QF contribution for data sample with missing momentum larger than cut point.

p_{FSI}^{lost}: How much percent of FSI events will be lost after applying missing momentum cut.

Summary

- First estimates for the polarization observables C_x, C_z, and P_y for the final-state interactions in $\overrightarrow{\gamma} d \rightarrow K^+ \overrightarrow{\Lambda} n$ were determined.

- One-fold, two-fold, and four-fold differential estimates were obtained.

- FSI and QF were separated, and the corresponding observables were extracted.

- Effect of FSI on the observables were studied.

- Data points of this work will be used to constrain free parameters of YN potentials and to extract a spin-average value of Λn scattering length.

Backup Slides

Data Analysis: Vertex Determination

Distance Of Closest Approach

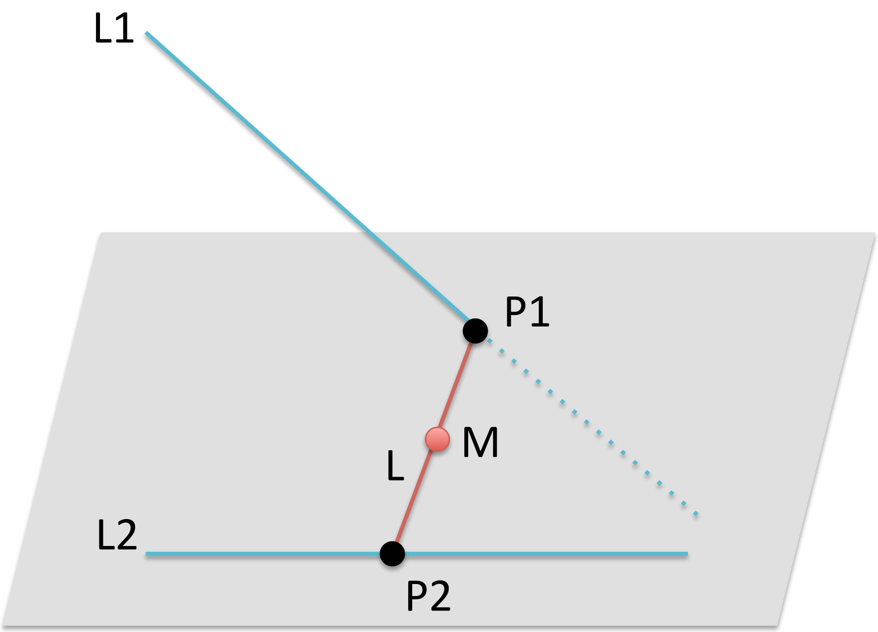

Vertex Cut

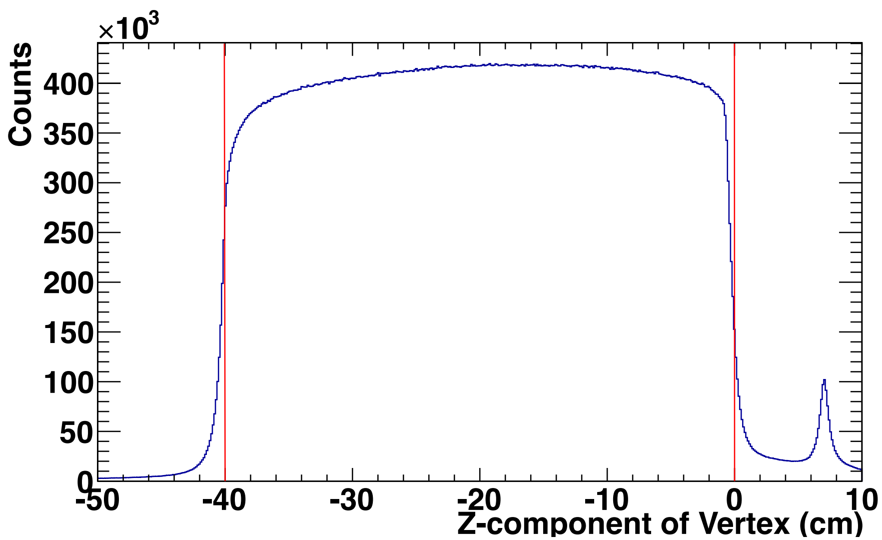

Data Analysis: Photon Polarization

The electron polarization for some special runs were measured by the Mϕller polarimeter.

The polarization of the photon beam was calculated using the Maximon and Olson relation

$$P_{cir} = \frac{E_\gamma(E + \frac{1}{3}E')P_e}{E^2 + E'^2 - \frac{2}{3}EE'}$$

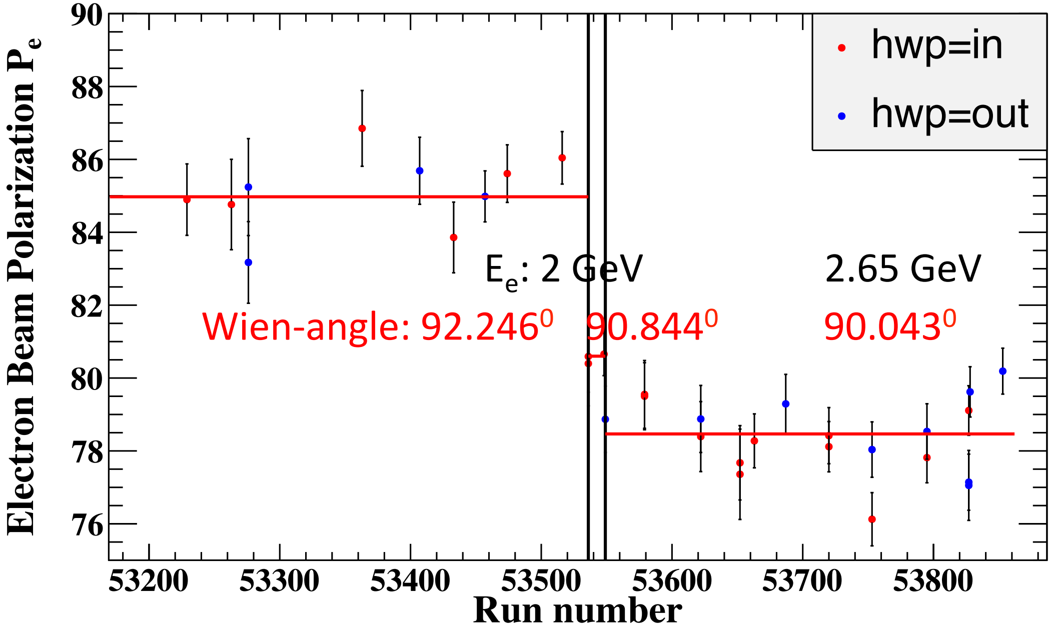

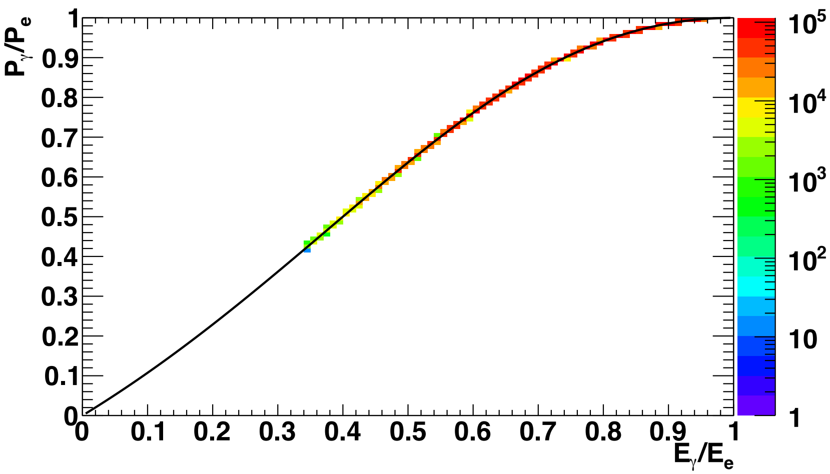

Background Subtraction: E_γ vs MM

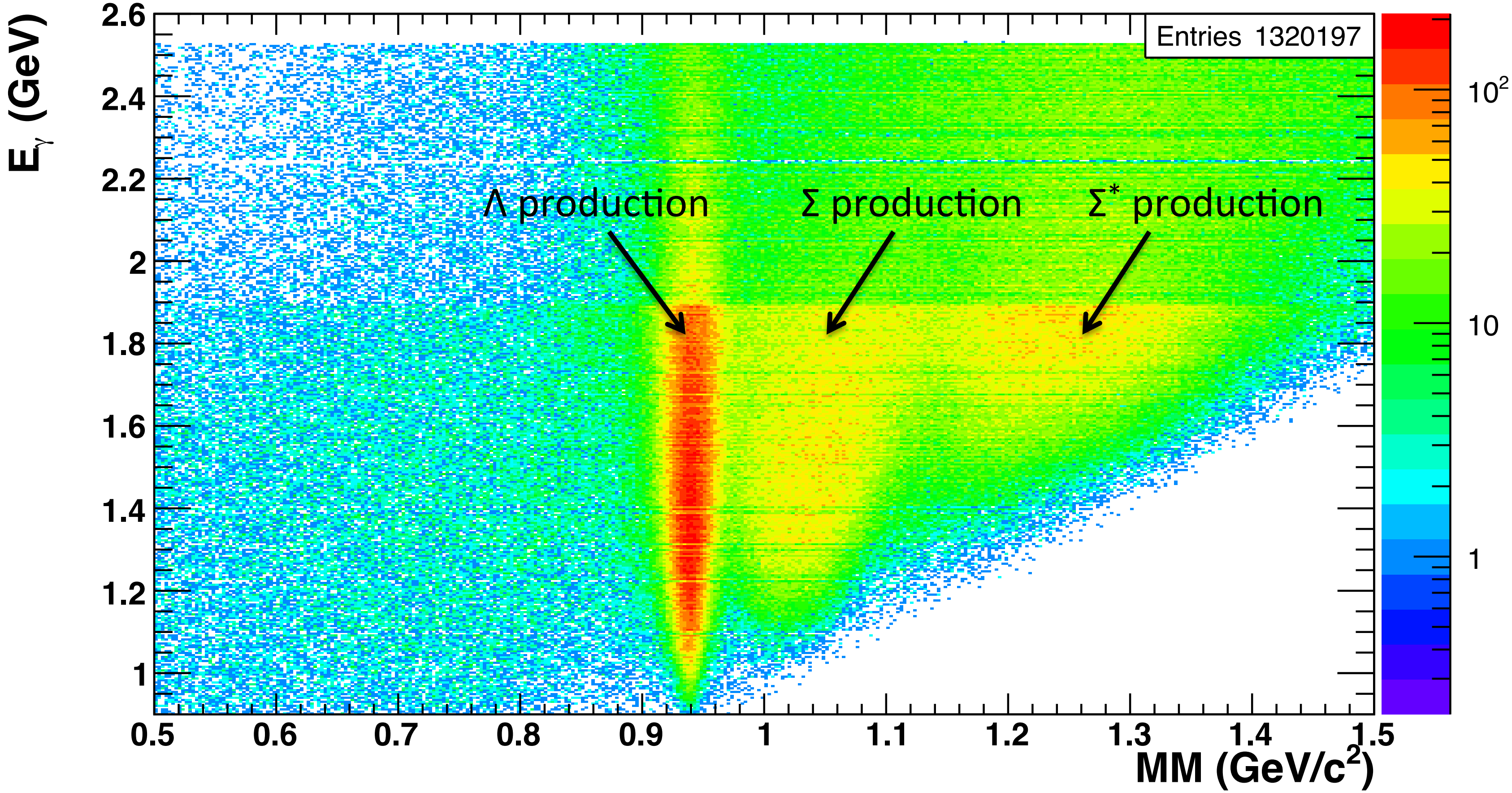

$$MM = \sqrt{(\widetilde{p}_\gamma + \widetilde{p}_d - \widetilde{p}_{K^+} - \widetilde{p}_p - \widetilde{p}_{\pi^-})^2}$$

Background Subtraction: Procedure of Simulation

- Generator for different channels

Channel	First step	Second step
Quasi-free for signal	$\gamma p \to K^+\Lambda$	n is spectator
π^0 mediated for signal	$\gamma n \to \pi^0 n$	$\pi^0 p \to K^+\Lambda$
π^+ mediated for signal	$\gamma p \to \pi^+ n$	$\pi^+ n \to K^+\Lambda$
Kn re-scattering for signal	$\gamma p \to K^+\Lambda$	$K^+ n \to K^+ n$
Λn re-scattering for signal	$\gamma p \to K^+\Lambda$	$\Lambda n \to \Lambda n$
Σn re-scattering for Σ production	$\gamma p \to K^+\Sigma$	$\Sigma n \to \Sigma n$
Quasi-free for Σ production	$\gamma p \to K^+\Sigma$	$\Sigma \to \Lambda\gamma$
Quasi-free for Σ^{*0} production	$\gamma p \to K^+\Sigma^{*0}$	$\Sigma^{*0} \to \Lambda\pi$
Quasi-free for Σ^{*-} production	$\gamma n \to K^+\Sigma^{*-}$	$\Sigma^{*-} \to \Lambda\pi^-$

- Raw data after generated data processed through GSIM
- Skimmed data after filtering raw data

Background Subtraction: Comparison Between Simulated and Real Data

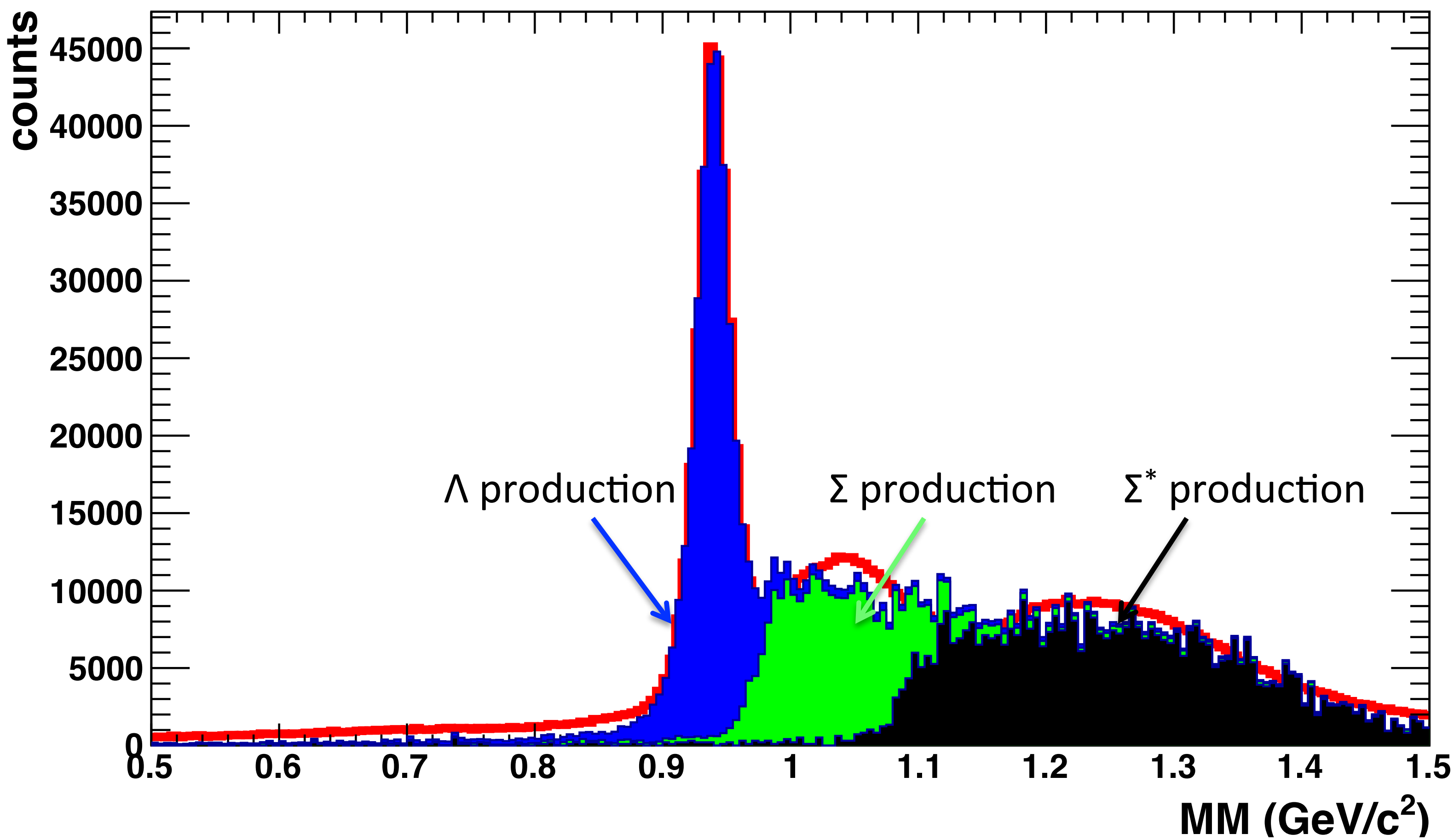

Background Subtraction: Distribution of Accidental Events

MM for different accidental tracks:

Accidental kaon: $\sqrt{(\tilde{p}_\gamma + \tilde{p}_d - \tilde{p}_{K_{acc}} - \tilde{p}_p - \tilde{p}_{\pi^-})^2}$

Accidental proton: $\sqrt{(\tilde{p}_\gamma + \tilde{p}_d - \tilde{p}_K - \tilde{p}_{p_{acc}} - \tilde{p}_{\pi^-})^2}$

Accidental pion: $\sqrt{(\tilde{p}_\gamma + \tilde{p}_d - \tilde{p}_K - \tilde{p}_p - \tilde{p}_{\pi^-_{acc}})^2}$

- The accidental track was produced randomly to replace the corresponding track of our reaction, such as kaon, proton and pion.
- The missing mass was then recalculated using the information of the accidental track.

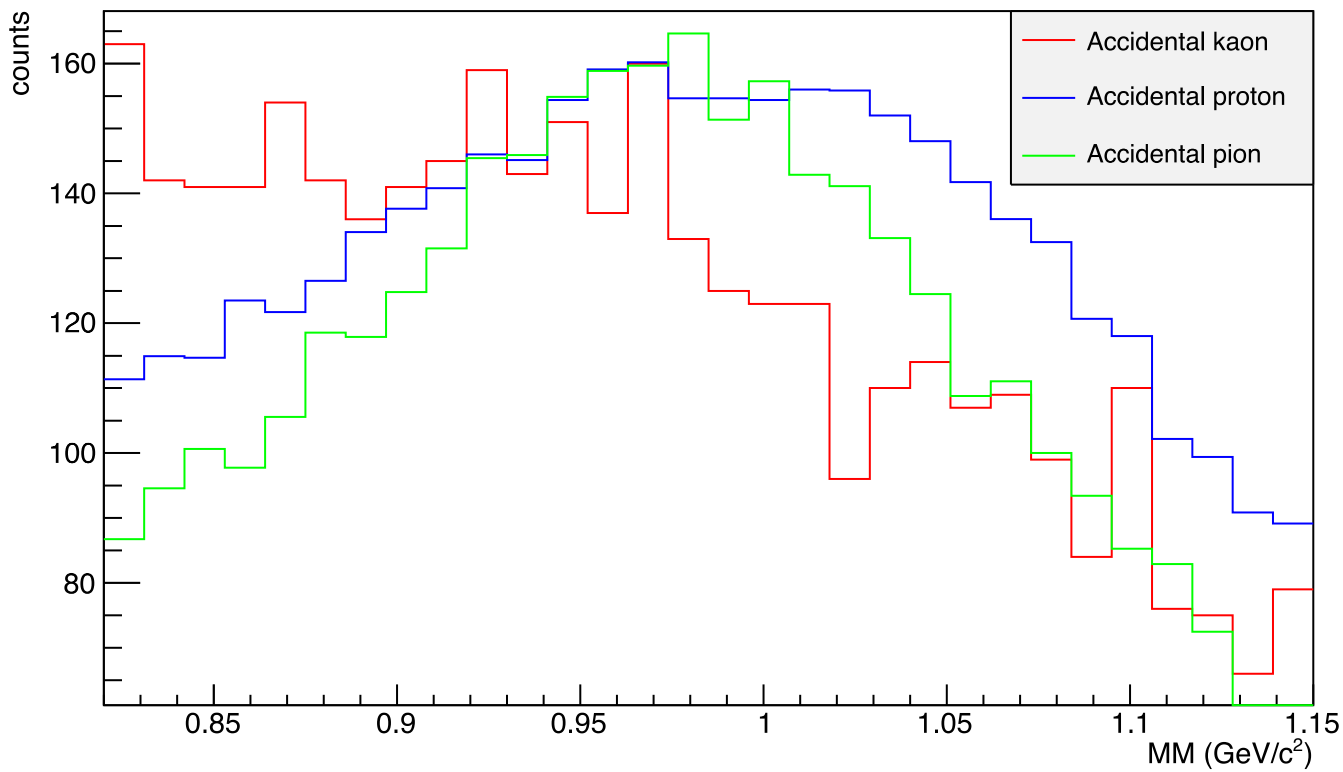

Background Subtraction: An Example for One Kinematic Bin

$$MM = \sqrt{(\widetilde{p}_\gamma + \widetilde{p}_d - \widetilde{p}_{K^+} - \widetilde{p}_p - \widetilde{p}_{\pi^-})^2}$$

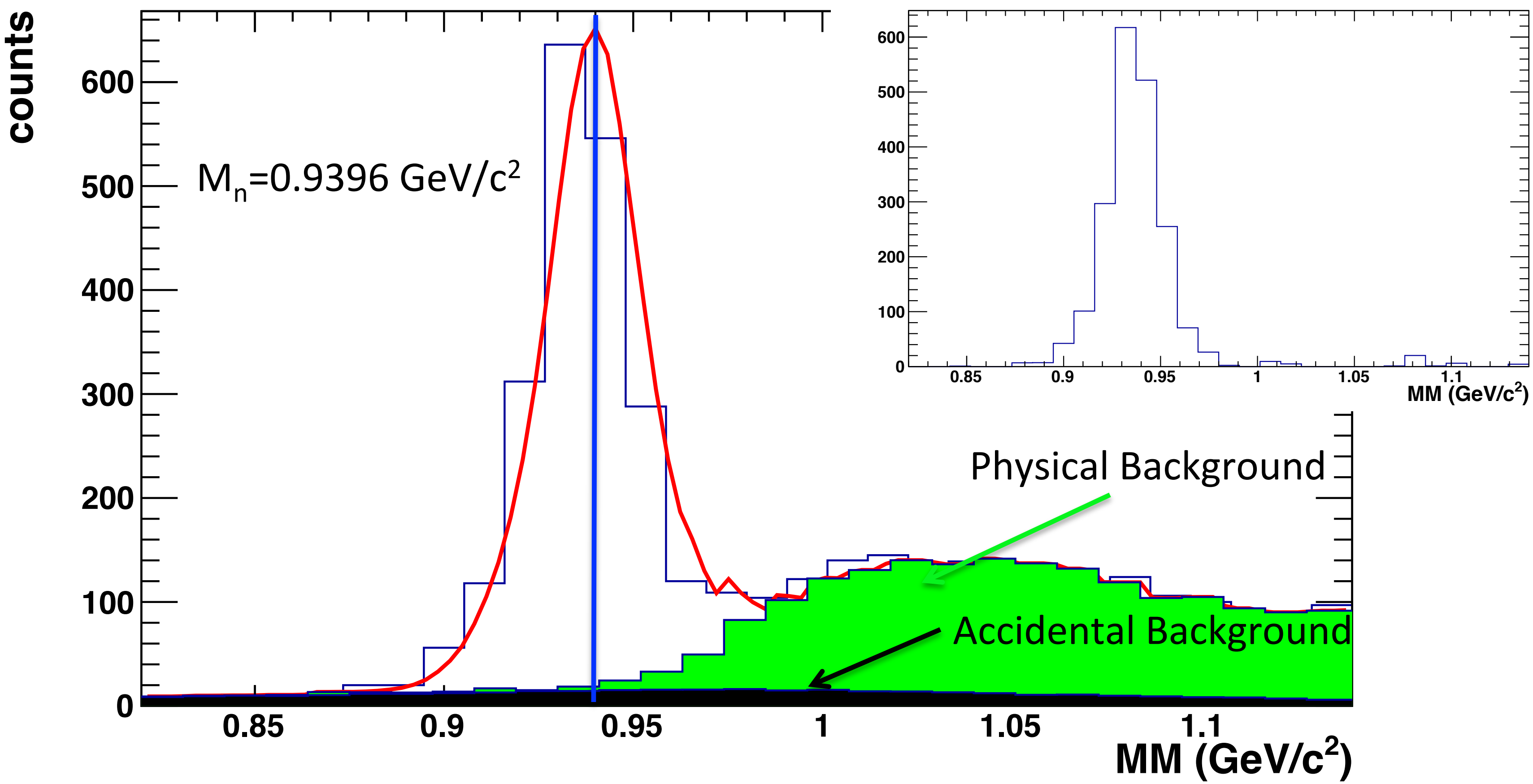

Extraction of C_x, C_z, and P_y

- The maximum likelihood method was used to extract the observables.

Probability density function defined from the polarized cross section:

$$L_i = c^{+,-}(1 \pm \alpha P_{circ} C_x \cos\theta_x \pm \alpha P_{circ} C_z \cos\theta_z + \alpha P_y \cos\theta_y)$$

Total likelihood is the product of the likelihoods for all individual events:

$$logL = b + \sum_{i=1}^{n^+} log[(1 + \alpha P^i_{circ} C_x \cos\theta^i_x + \alpha P^i_{circ} C_z \cos\theta^i_z + \alpha P_y \cos\theta^i_y) w^i]$$

$$\sum_{j=1}^{n^-} log[(1 - \alpha P^j_{circ} C_x \cos\theta^j_x - \alpha P^j_{circ} C_z \cos\theta^j_z + \alpha P_y \cos\theta^j_y) w^j]$$

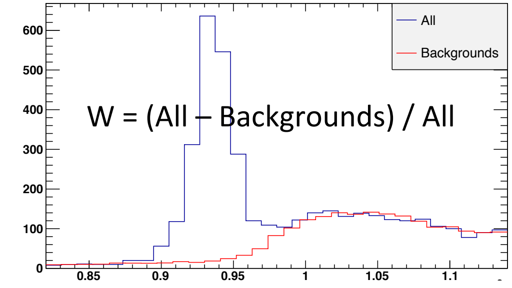

- The maximum likelihood method has advantages compared to binned methods.
  - Simultaneous extraction of polarization observables.
  - Reliable extraction even with a small number of events.
  - Bias is negligibly small, while bias of observables extracted from a binned method is much larger.

Extraction of C_x, C_z, and P_y

The maximum likelihood method was used to extract the observables.

Probability density function defined from the polarized cross section:

$$L_i = c^{+,-}(1 \pm \alpha P_{circ} C_x \cos\theta_x \pm \alpha P_{circ} C_z \cos\theta_z + \alpha P_y \cos\theta_y)$$

Total likelihood is the product of the likelihoods for all individual events:

$$logL = b + \sum_{i=1}^{n^+} log[(1 + \alpha P^i_{circ} C_x \cos\theta^i_x + \alpha P^i_{circ} C_z \cos\theta^i_z + \alpha P_y \cos\theta^i_y)w^i]$$

$$\sum_{j=1}^{n^-} log[(1 - \alpha P^j_{circ} C_x \cos\theta^j_x - \alpha P^j_{circ} C_z \cos\theta^j_z + \alpha P_y \cos\theta^j_y)w^j]$$

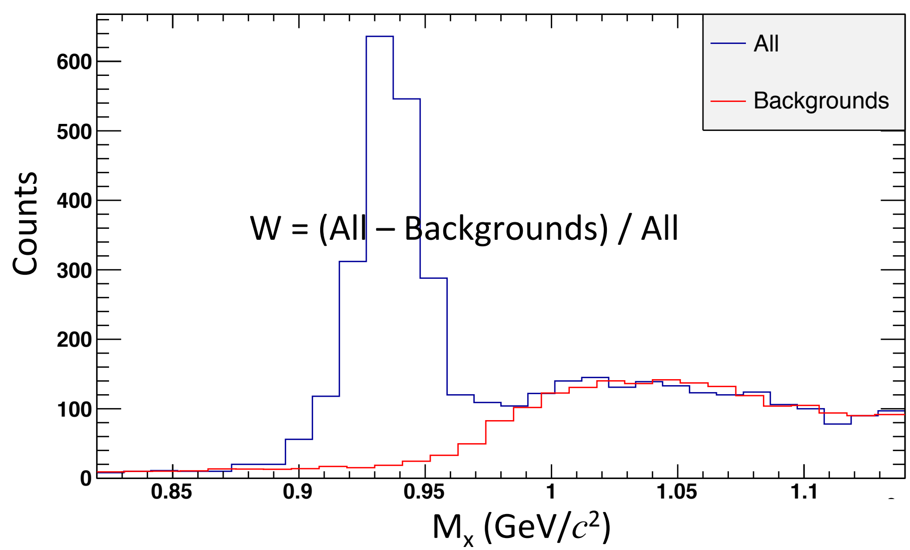

Observable-Extraction Methods

- One-dimensional fit:

$$Asym = \frac{Y^+ - Y^-}{Y^+ + Y^-} = \frac{\int\int \frac{d\sigma^+}{d\Omega} d(cos\theta_y) d(\cos\theta_{z/x}) - \int\int \frac{d\sigma^-}{d\Omega} d(cos\theta_y) d(\cos\theta_{z/x})}{\int\int \frac{d\sigma^+}{d\Omega} d(cos\theta_y) d(\cos\theta_{z/x}) + \int\int \frac{d\sigma^-}{d\Omega} d(cos\theta_y) d(\cos\theta_{z/x})} = \alpha P_{circ} C_{x/z} \cos\theta_{x/z}$$

- Two-dimensional fit:

$$Asym = \frac{Y^+ - Y^-}{Y^+ + Y^-} = \frac{\int \frac{d\sigma^+}{d\Omega} d(cos\theta_y)) - \int \frac{d\sigma^-}{d\Omega} d(cos\theta_y)}{\int \frac{d\sigma^+}{d\Omega} d(cos\theta_y)) + \int \frac{d\sigma^-}{d\Omega} d(cos\theta_y)} = \alpha P_{circ} C_x \cos\theta_x + \alpha P_{circ} C_z \cos\theta_z$$

- Maximum likelihood Method:

$$PDF = \frac{d\sigma}{d\Omega}_{|unpol} (1 \pm \alpha P_{circ} C_x \cos\theta_x \pm \alpha P_{circ} C_z \cos\theta_z + \alpha P_y \cos\theta_y)$$

Results for C_x and C_z from Different Methods

$\cos\theta_K$: [0.35, 0.55]

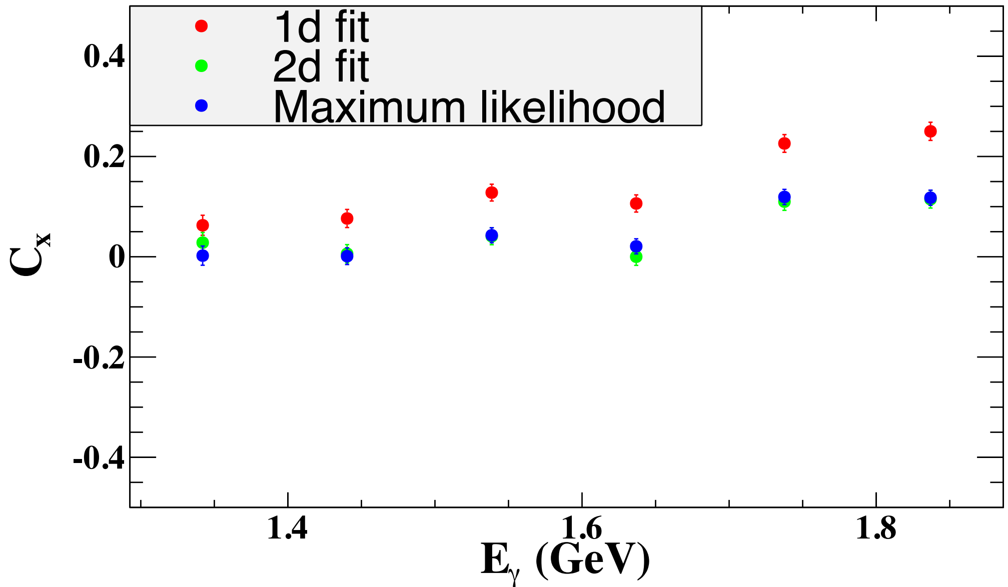

$\cos\theta_K$: [0.35, 0.55]

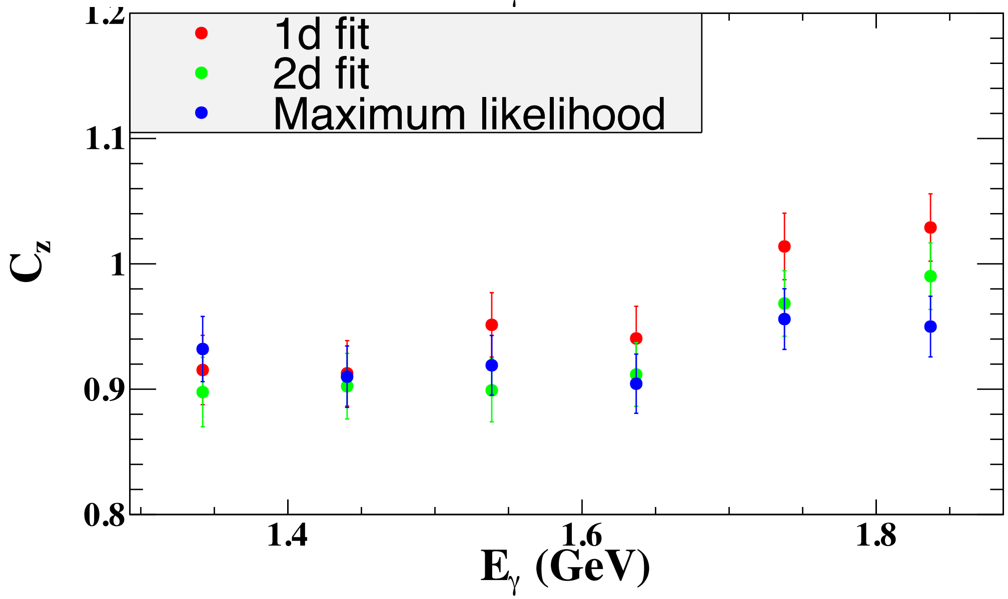

Comparison With g1c Results

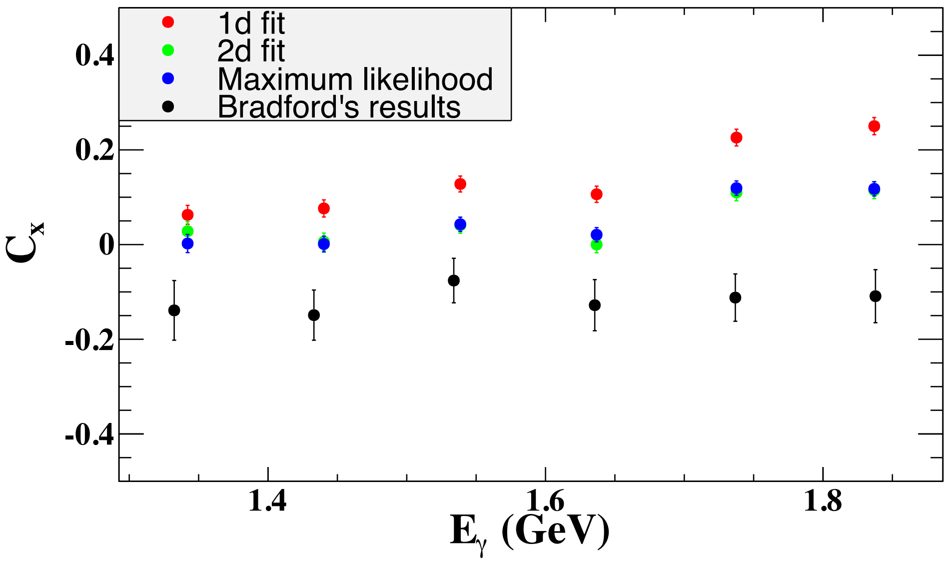

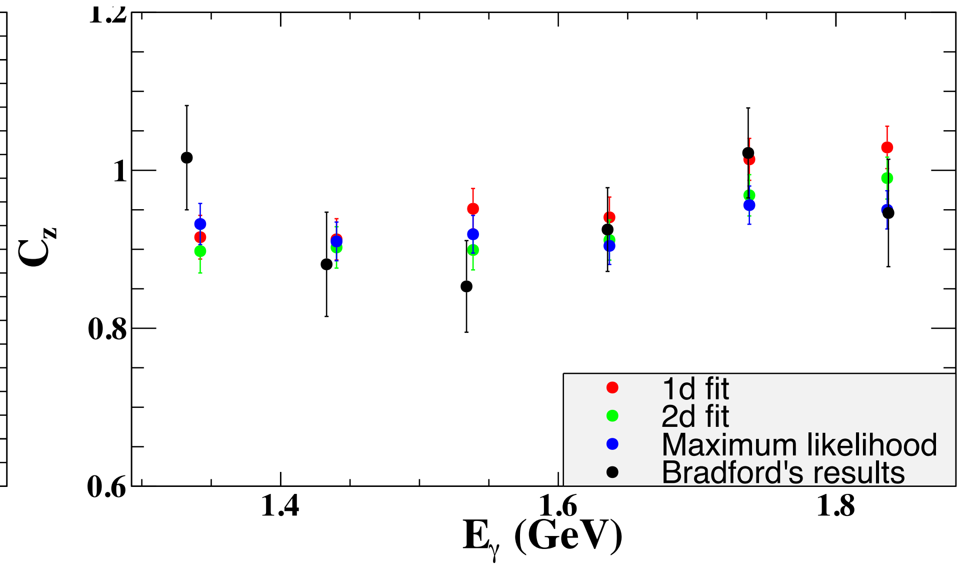

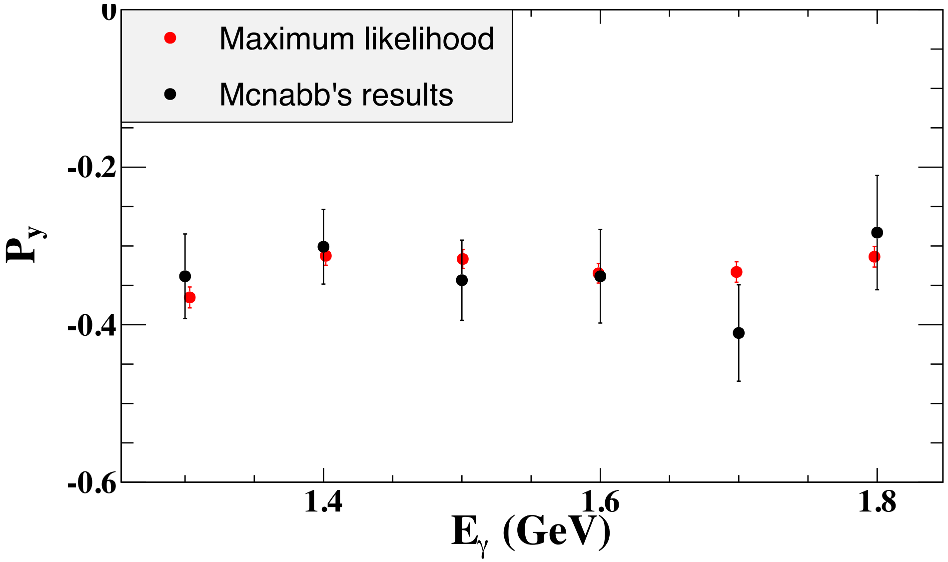

$\cos\theta_K$: [0.35, 0.55]

C_x and C_z from Robert K. Bradford
P_y from John W.C. McNabb

- Dataset: g1c
- Reaction: $\overrightarrow{\gamma} p \rightarrow K^+ \overrightarrow{\Lambda}$

Simulation Study to Understand Different Methods

A study was used to evaluate potential bias of the maximum likelihood method and the binned methods.

- 6000 different experiments, with 10^6 events in each experiment, were generated according to the differential polarized cross section with realistic values of C_x, C_z, and P_y for $\vec{\gamma} p \to K^+ \vec{\Lambda}$.
- Generated data were processed through GSIM and gpp.
- After raw data were skimmed, the observables were extracted using the maximum likelihood method and the binned methods.

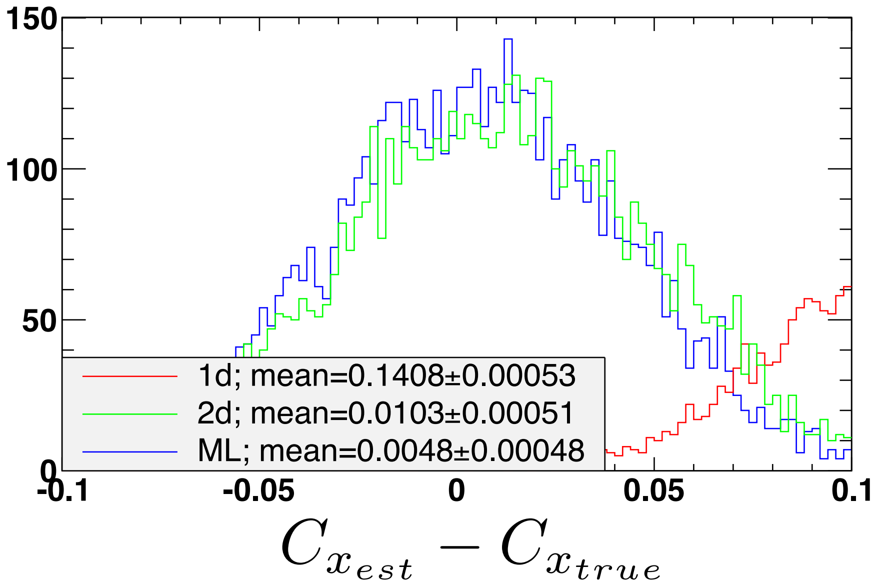

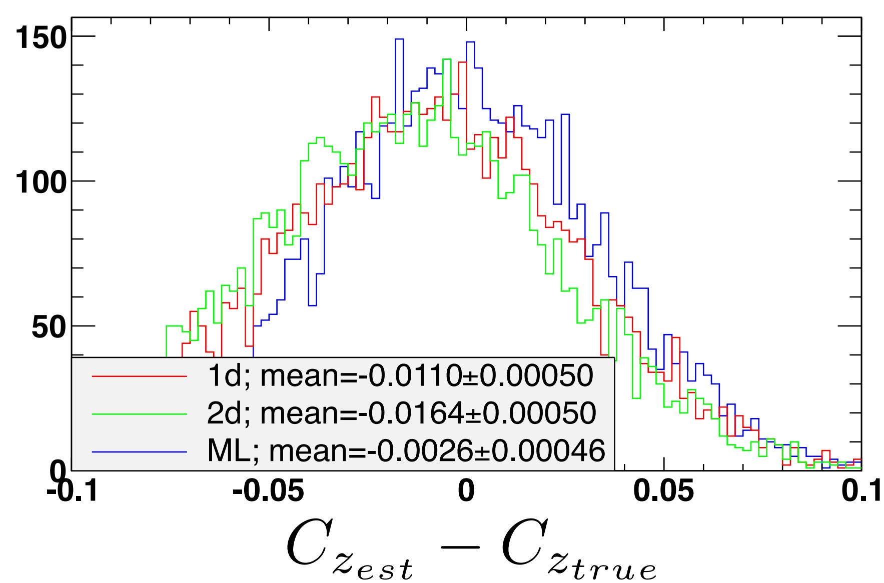

Simulation Study to Compare Different Methods

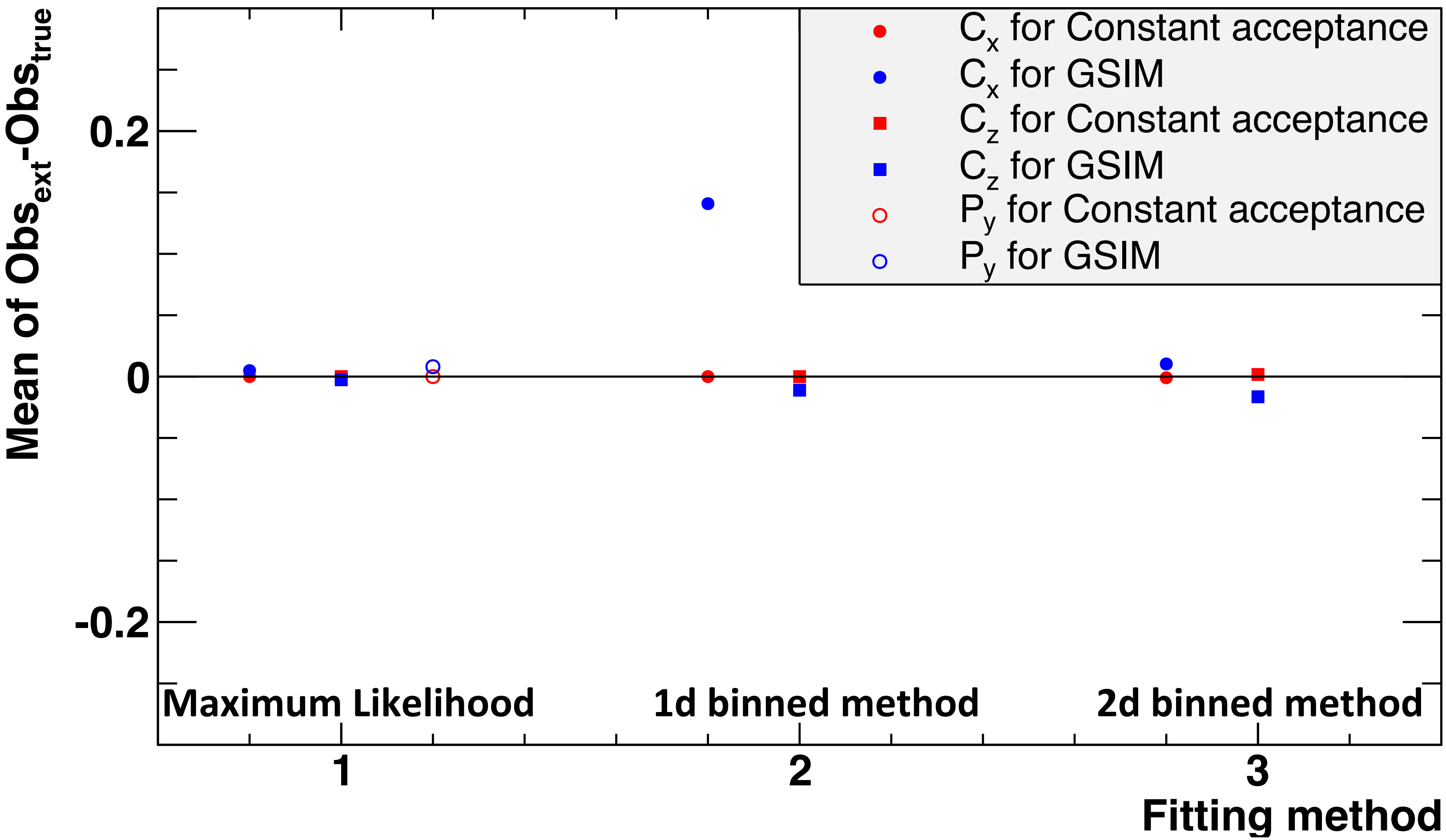

Examples of 1D Fit

E_γ: [1.5875, 1.6875] GeV and $\cos\theta_K$: [0.35, 0.55]

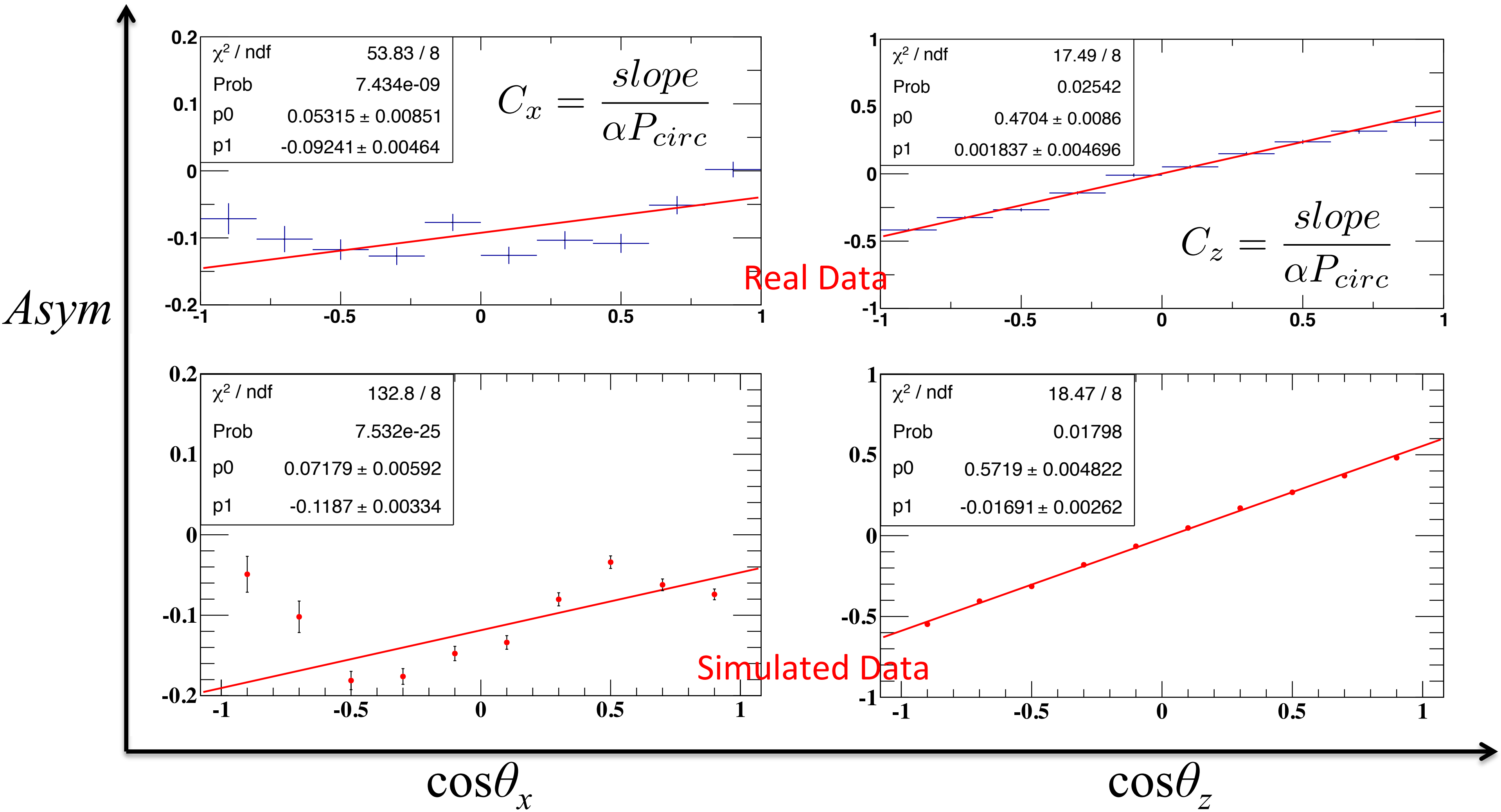

Why is the Bias Small for C_z from 1D Fit?

In the spherical coordinate system:

$$\begin{cases} \cos\theta_x = \sin\theta\cos\phi \\ \cos\theta_y = \sin\theta\sin\phi \\ \cos\theta_z = \cos\theta \end{cases}$$

$$\cos^2\theta_x + \cos^2\theta_y + \cos^2\theta_z = 1$$

θ_x, θ_y, and θ_z are not independent.

Event yield: $Y^{\pm}(\theta,\phi) = N_\gamma^{\pm} N_T \sigma^{\pm}(\theta,\phi) A(\theta,\phi)$

Integral over ϕ: $Y^{\pm}(\theta) = c(A(\theta) \pm \alpha P_{circ} C_x \sin\theta A_x(\theta) \pm \alpha P_{circ} C_z \cos\theta A(\theta) + \alpha P_y \sin\theta A_y(\theta))$

$$A(\theta) = \int_0^{2\pi} A(\theta,\phi)\,\mathrm{d}\phi;\ \ A_x(\theta) = \int_0^{2\pi} A(\theta,\phi)\cos\phi\,\mathrm{d}\phi;\ \ A_y(\theta) = \int_0^{2\pi} A(\theta,\phi)\sin\phi\,\mathrm{d}\phi$$

$$A_x(\theta) = \int_0^{2\pi} A(\theta,\phi)\cos\phi\,\mathrm{d}\phi < \int_0^{2\pi} A(\theta,\phi)|\cos\phi|\,\mathrm{d}\phi < |\cos\phi|_{max}\int_0^{2\pi} A(\theta,\phi)\,\mathrm{d}\phi = \int_0^{2\pi} A(\theta,\phi)\,\mathrm{d}\phi = A(\theta)$$

Asymmetry: $Asym = \dfrac{Y^+ - Y^-}{Y^+ + Y^-} = \dfrac{\alpha P_{circ} C_x \sin\theta A_x(\theta) + \alpha P_{circ} C_z \cos\theta A(\theta)}{A(\theta) + \alpha P_y \sin\theta A_y(\theta)}$

Generally, $|C_x| << |C_z|, |P_y| < |C_z|$

Therefore, $Asym \approx \alpha P_{circ} C_z \cos\theta_z$

Why is the Bias Large for C_x from 1D Fit?

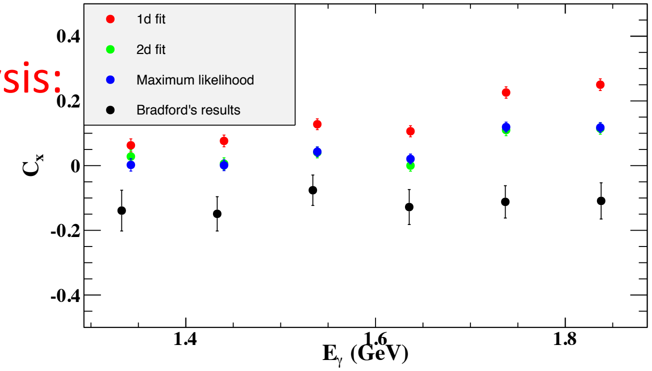

Spherical coordinate system for the convenience of C_x analysis:

$$
\begin{cases}
\cos\theta_x = \cos\theta \\
\cos\theta_y = \sin\theta\cos\phi \\
\cos\theta_z = \sin\theta\sin\phi
\end{cases}
$$

Asymmetry: $$Asym = \frac{Y^+ - Y^-}{Y^+ + Y^-} = \frac{\alpha P_{circ} C_x \cos\theta A(\theta) + \alpha P_{circ} C_z \sin\theta A_z(\theta)}{A(\theta) + \alpha P_y \sin\theta A_y(\theta)}$$

In general, C_x is small relative to C_z and P_y, so C_z and P_y terms do not cancel. Therefore, the asymmetry for C_x is not a linear function of $\cos\theta_x$.

- The effect of acceptance cannot be ignored in 1D fit, especially for C_x.
- The situation with P_y is somewhat in-between C_x and C_z if it's extracted by 1D fit.
- 2D fitting can reduce the effect of the acceptance to some extent.

Effect of Missing Momentum Cut

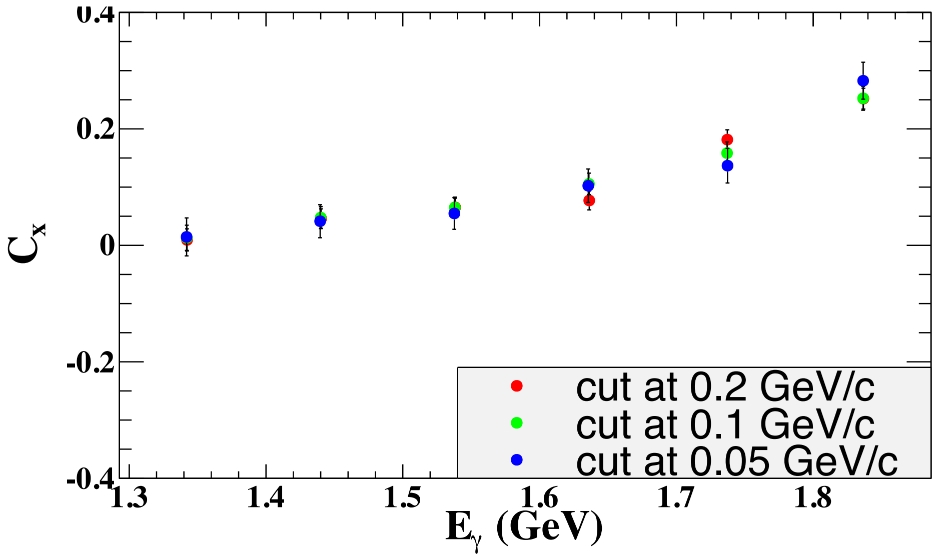

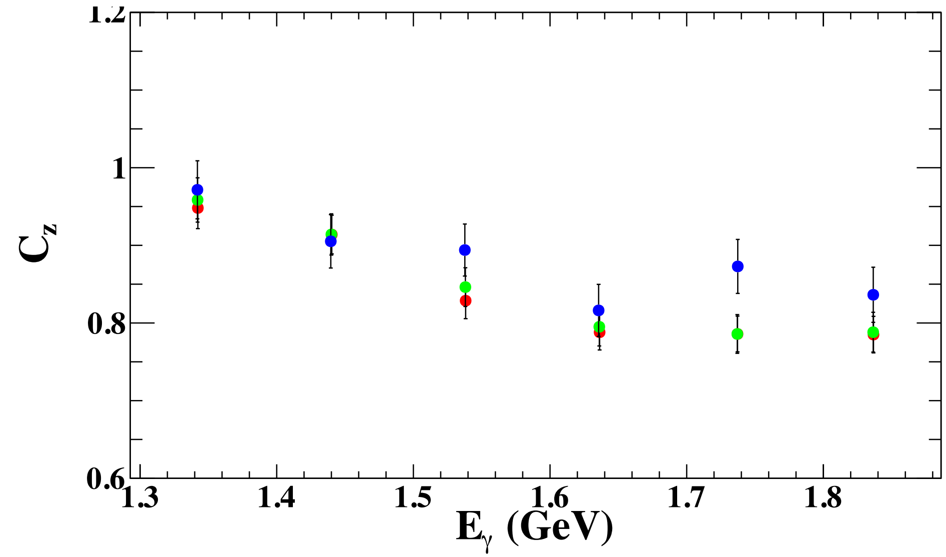

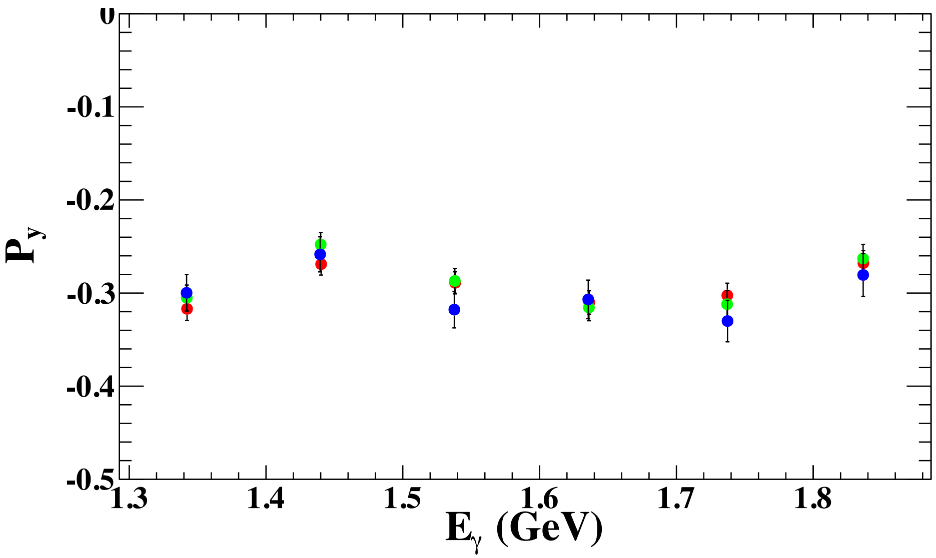

$\cos\theta_K$: [0.15, 0.35]

The missing momentum was cut at points 0.2, 0.1 and 0.05 GeV/c.

Results: Axis Convention of the Quasi-free Mechanism

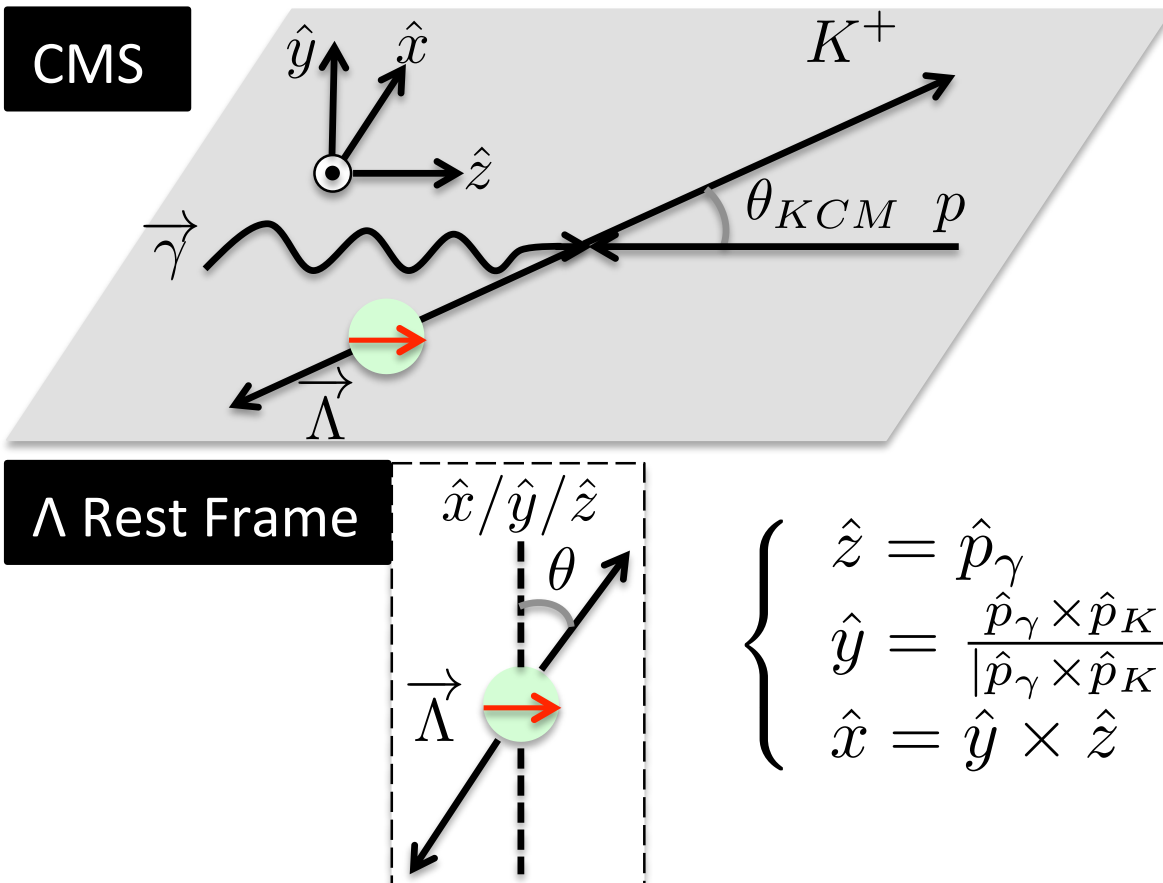

$$\begin{cases} \hat{z} = \hat{p}_\gamma \\ \hat{y} = \dfrac{\hat{p}_\gamma \times \hat{p}_K}{|\hat{p}_\gamma \times \hat{p}_K|} \\ \hat{x} = \hat{y} \times \hat{z} \end{cases}$$

Results: Results for the Quasi-free Mechanism

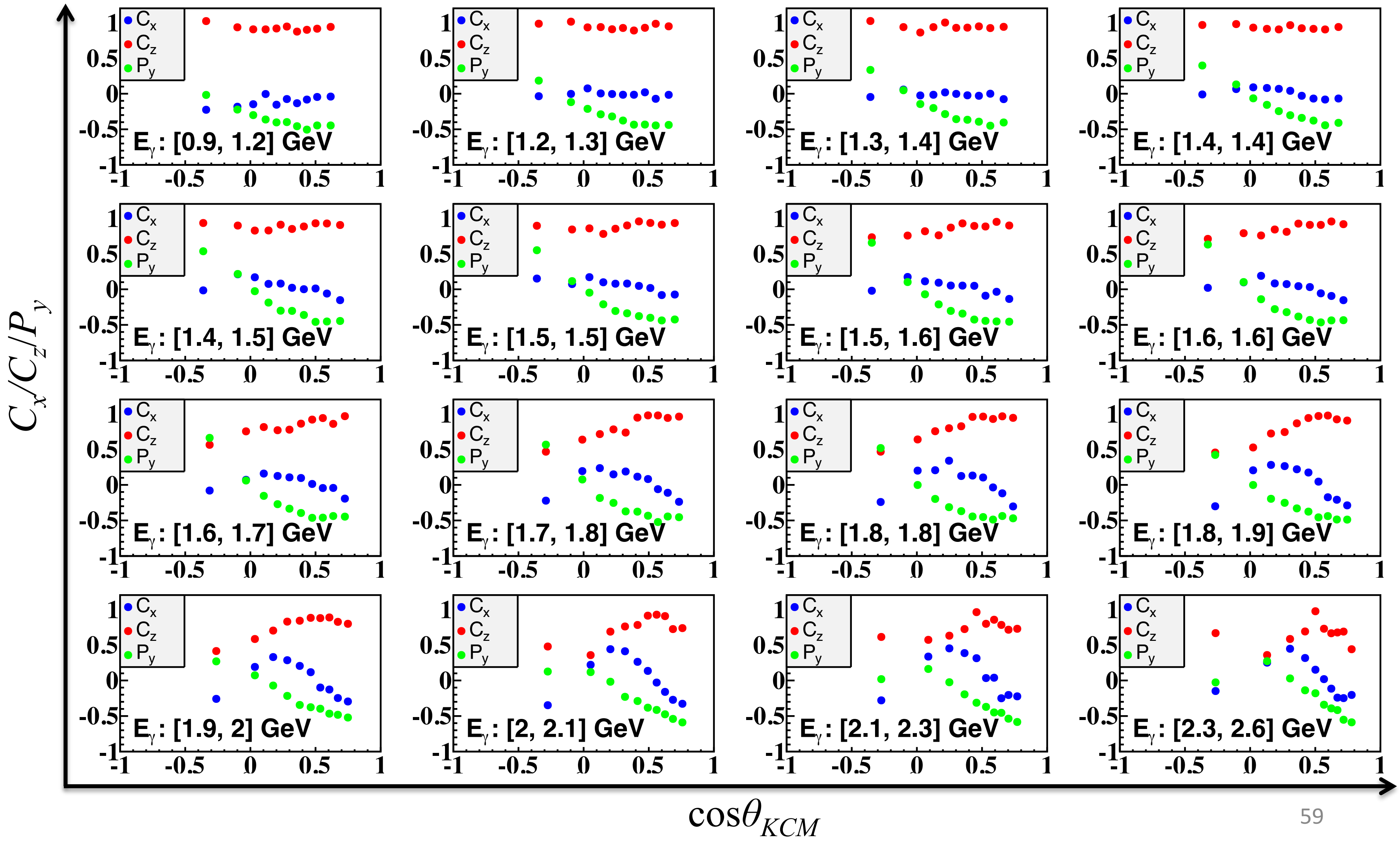

Results: One-fold Differential Estimate of C_x for the Final-State Interactions

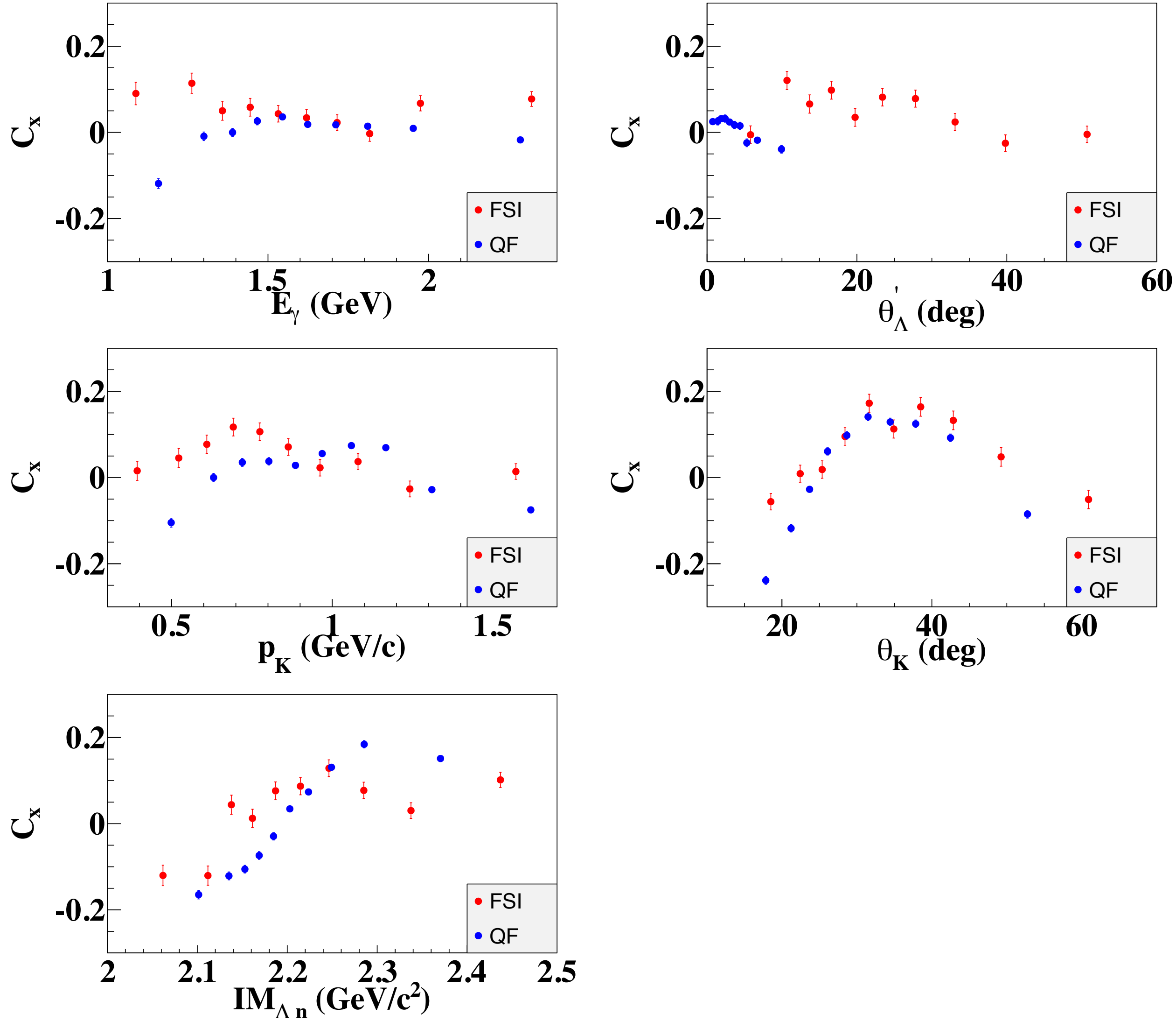

Results: One-fold Differential Estimate of C_z for the Final-State Interactions

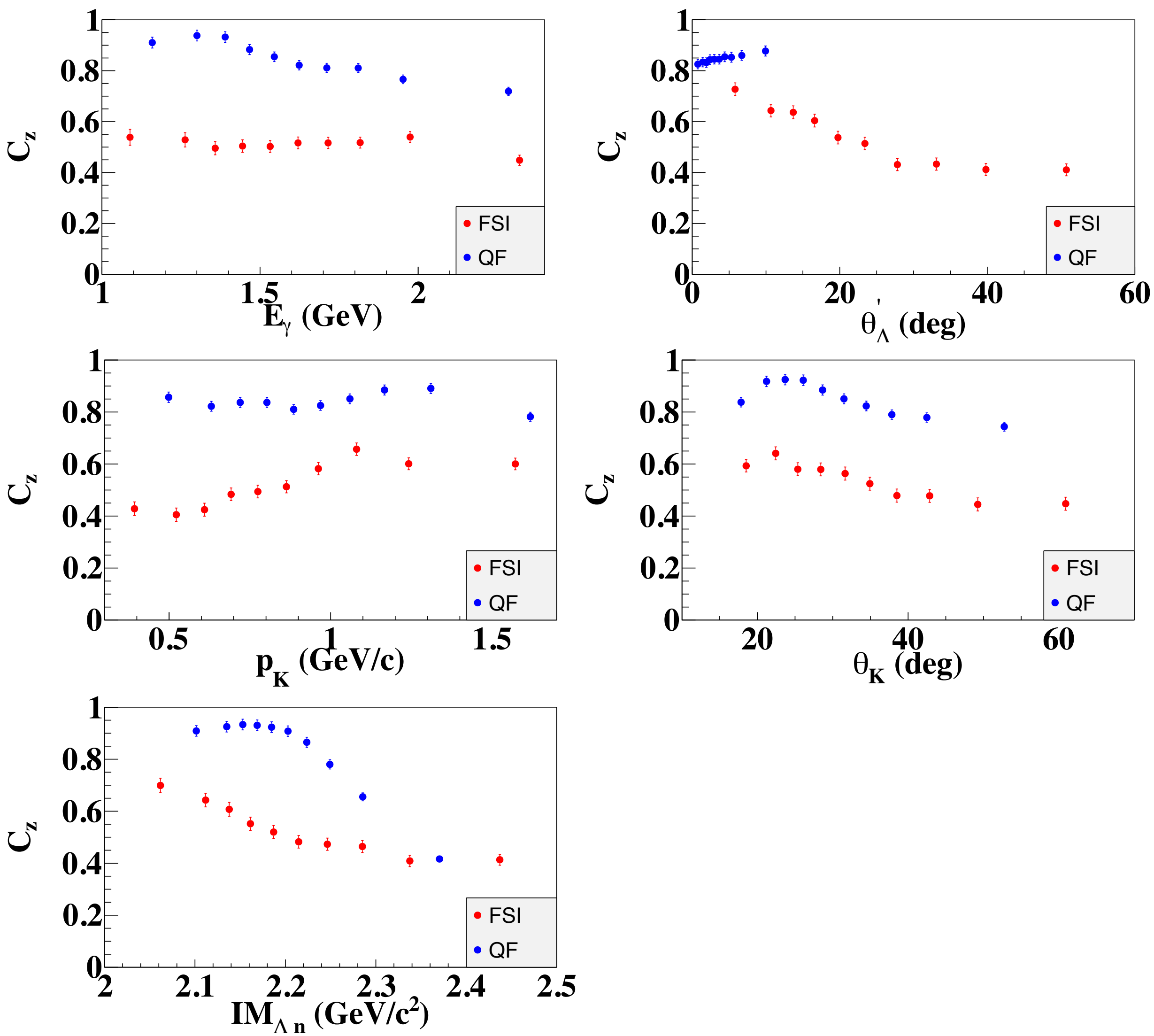

Results: One-fold Differential Estimate of P_y for the Final-State Interactions

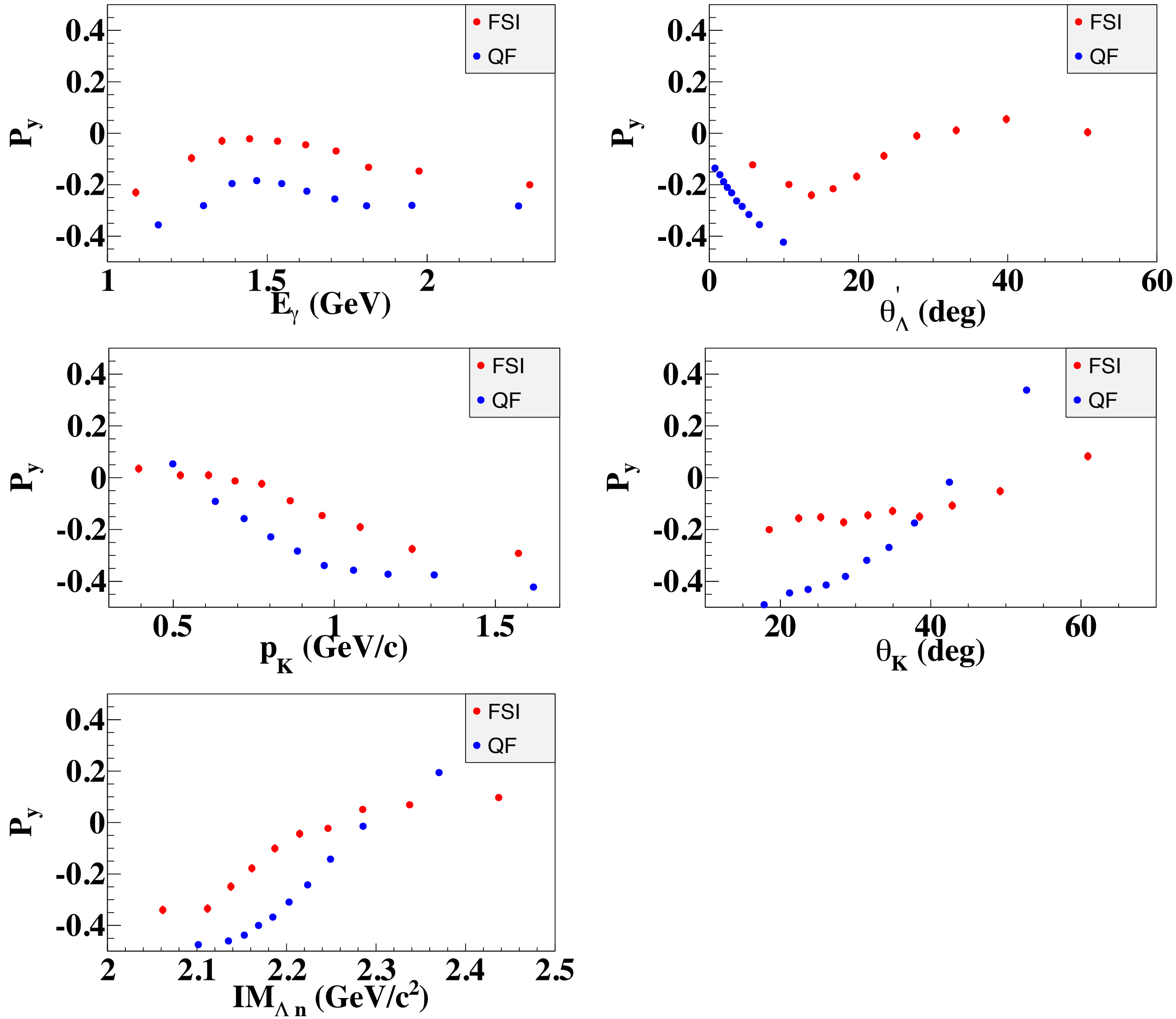

Two-fold differential estimates
$C_x(E_\gamma, \theta'_\Lambda)$, $C_z(E_\gamma, \theta'_\Lambda)$, and $P_y(E_\gamma, \theta'_\Lambda)$

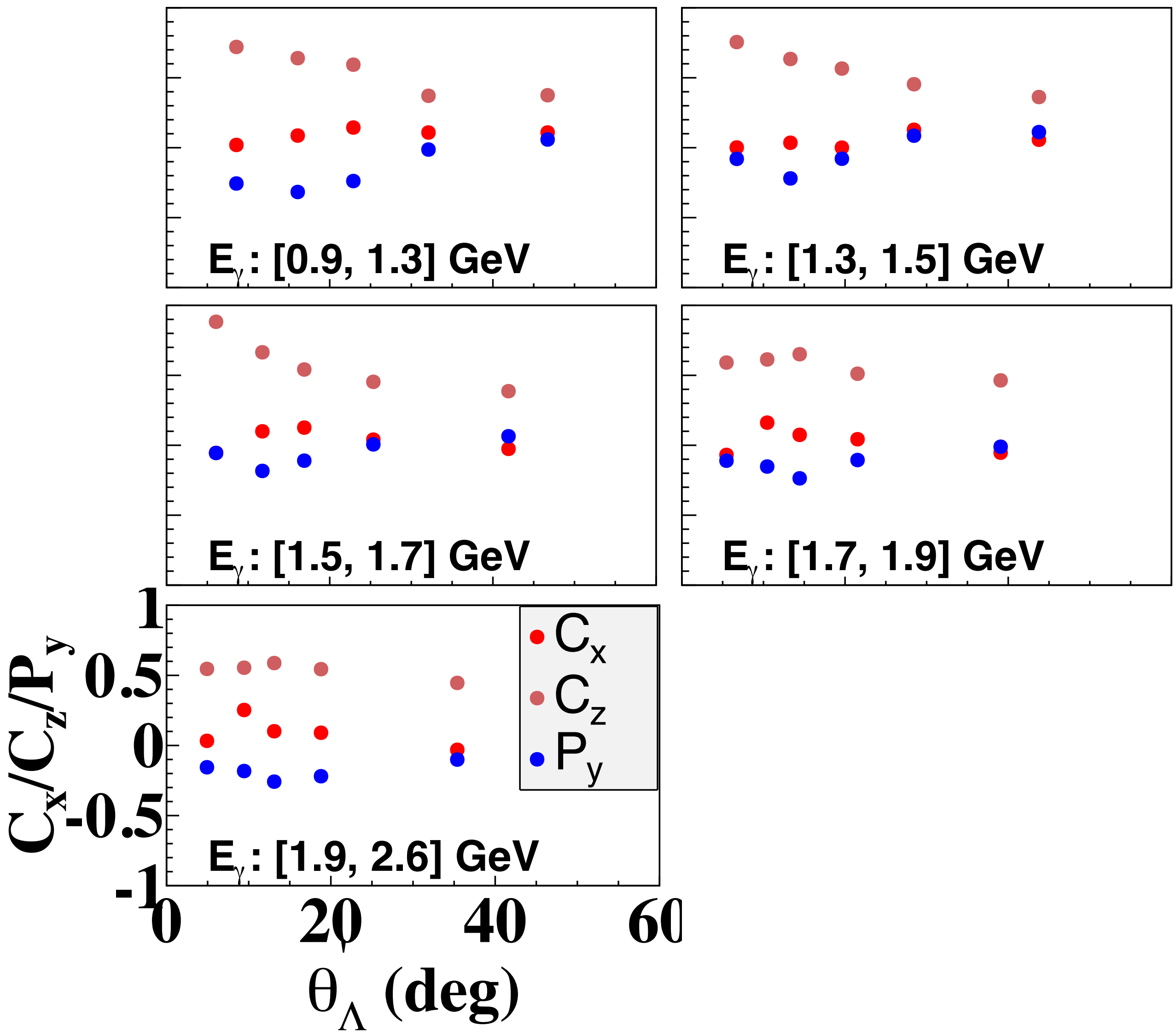

Results: Two-fold differential estimates $C_x(p_K, \theta'_\Lambda)$, $C_z(p_K, \theta'_\Lambda)$, and $P_y(p_K, \theta'_\Lambda)$

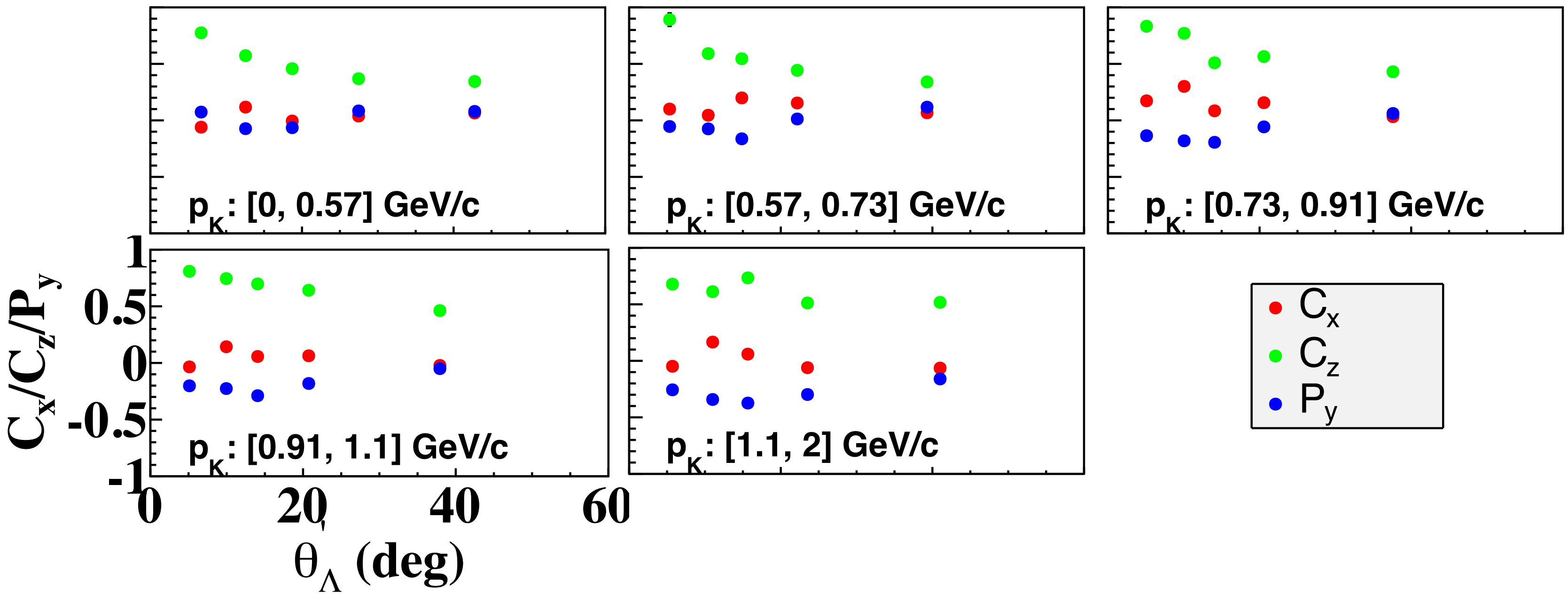

Results: Two-fold differential estimates $C_x(\theta_K, \theta'_\Lambda)$, $C_z(\theta_K, \theta'_\Lambda)$, and $P_y(\theta_K, \theta'_\Lambda)$

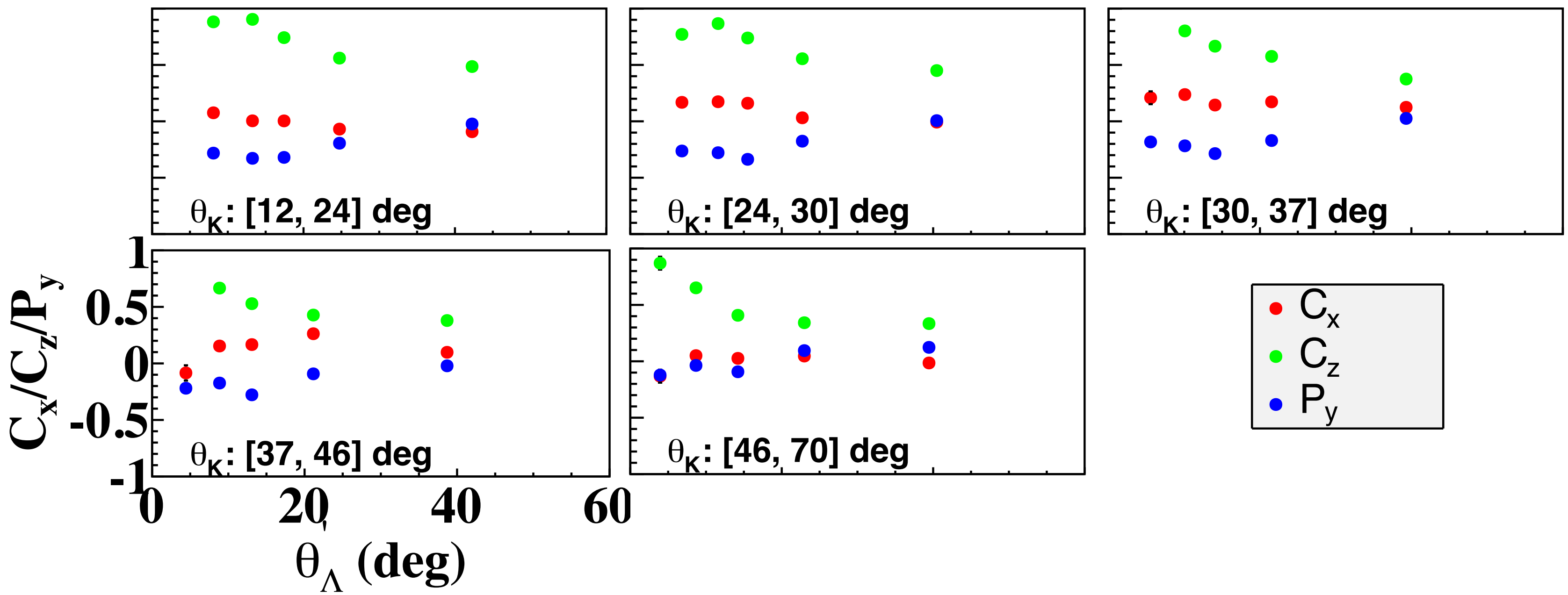

Results: Two-fold differential estimates Bin Setup in E_γ and θ'_Λ

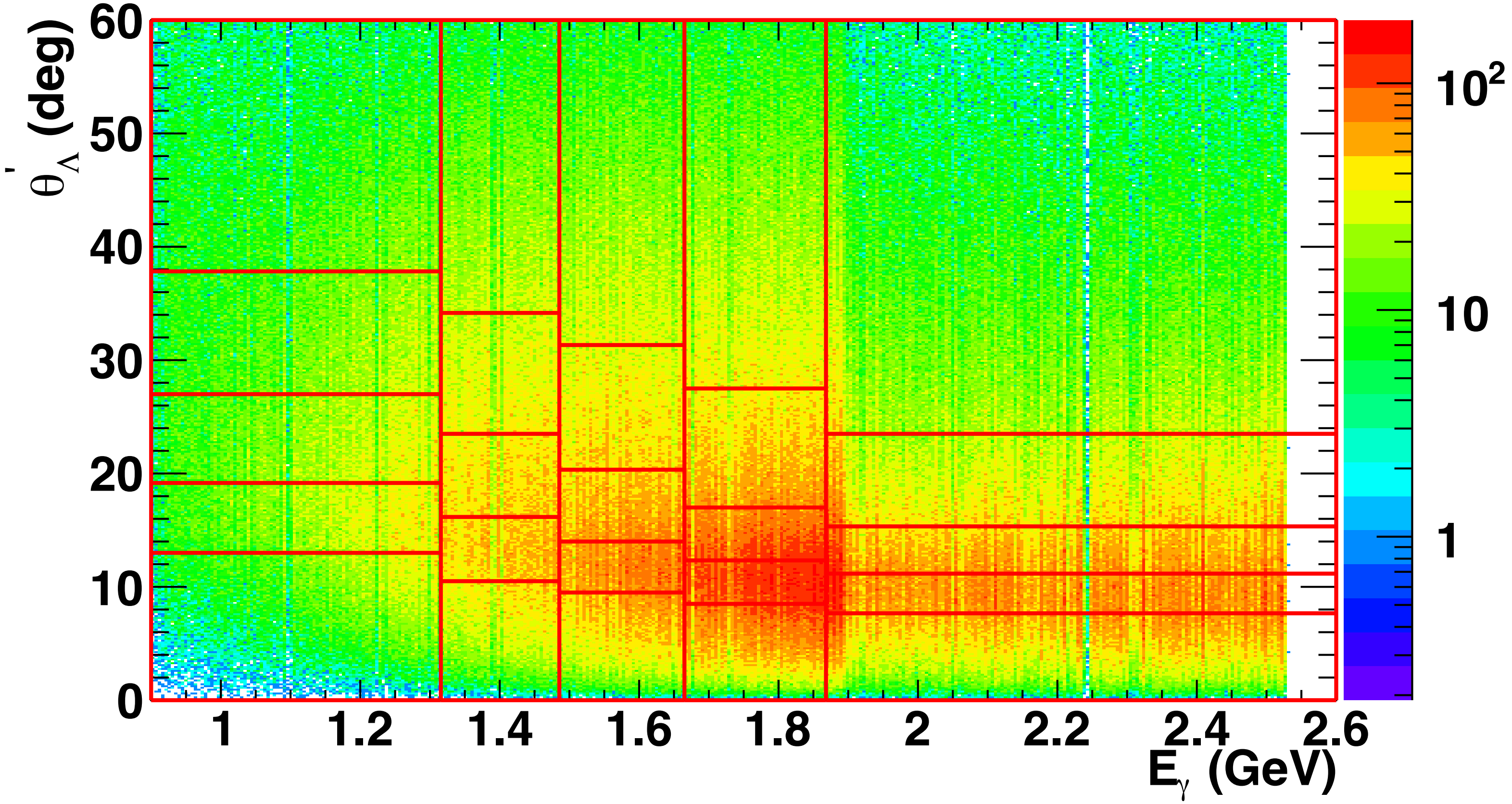

Discussion: Effect of Missing Momentum Cut

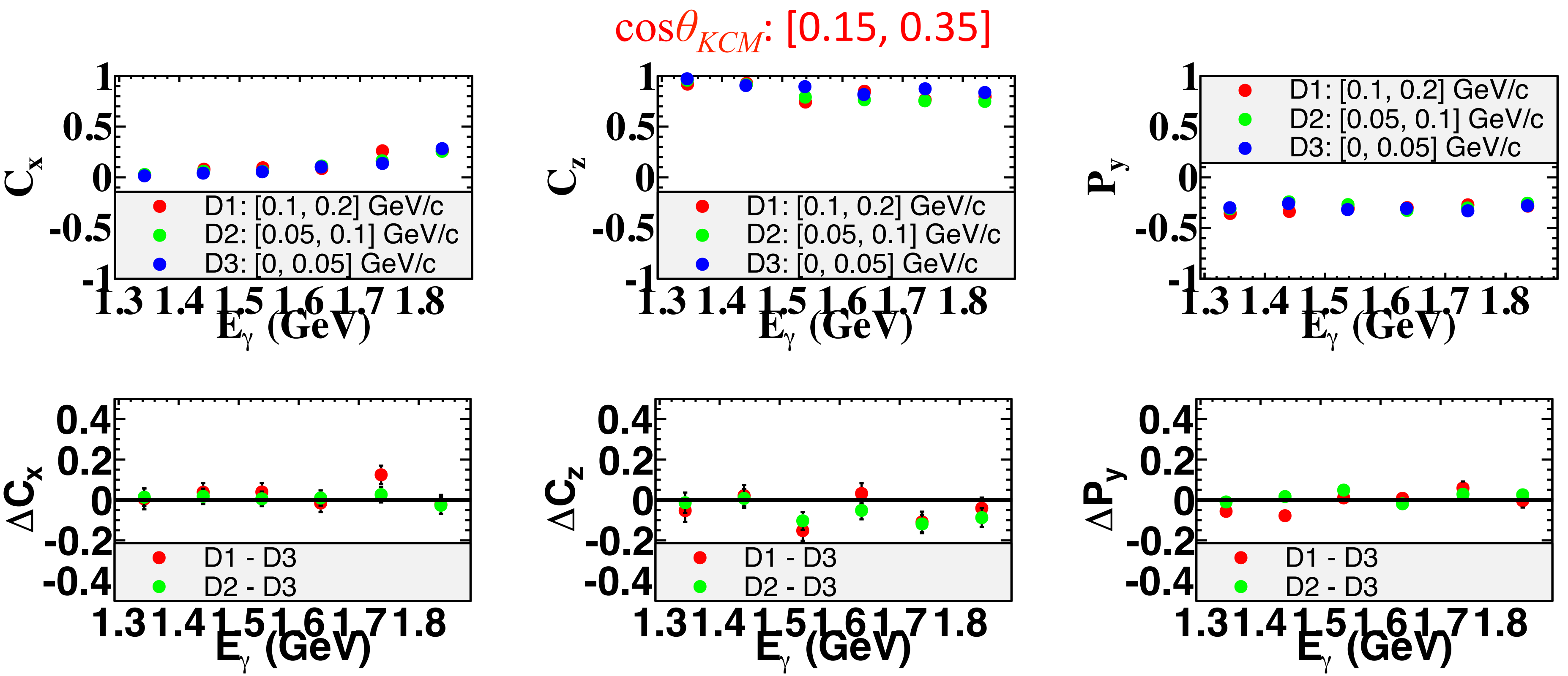

The missing momentum is cut within different ranges: 0.2 − 0.1 GeV/c, 0.05 – 0.1 GeV/c, and 0 – 0.05 GeV/c.

Discussion: Examples of 1D Fit

$$Asym = \frac{Y^+ - Y^-}{Y^+ + Y^-} = \frac{\int\int \frac{d\sigma^+}{d\Omega} d(cos\theta_y) d(\cos\theta_{z/x}) - \int\int \frac{d\sigma^-}{d\Omega} d(cos\theta_y) d(\cos\theta_{z/x})}{\int\int \frac{d\sigma^+}{d\Omega} d(cos\theta_y) d(\cos\theta_{z/x}) + \int\int \frac{d\sigma^-}{d\Omega} d(cos\theta_y) d(\cos\theta_{z/x})} = \alpha P_{circ} C_{x/z} \cos\theta_{x/}$$

E_γ: [1.5875, 1.6875] GeV and cosθ_{KCM}: [0.35, 0.55]

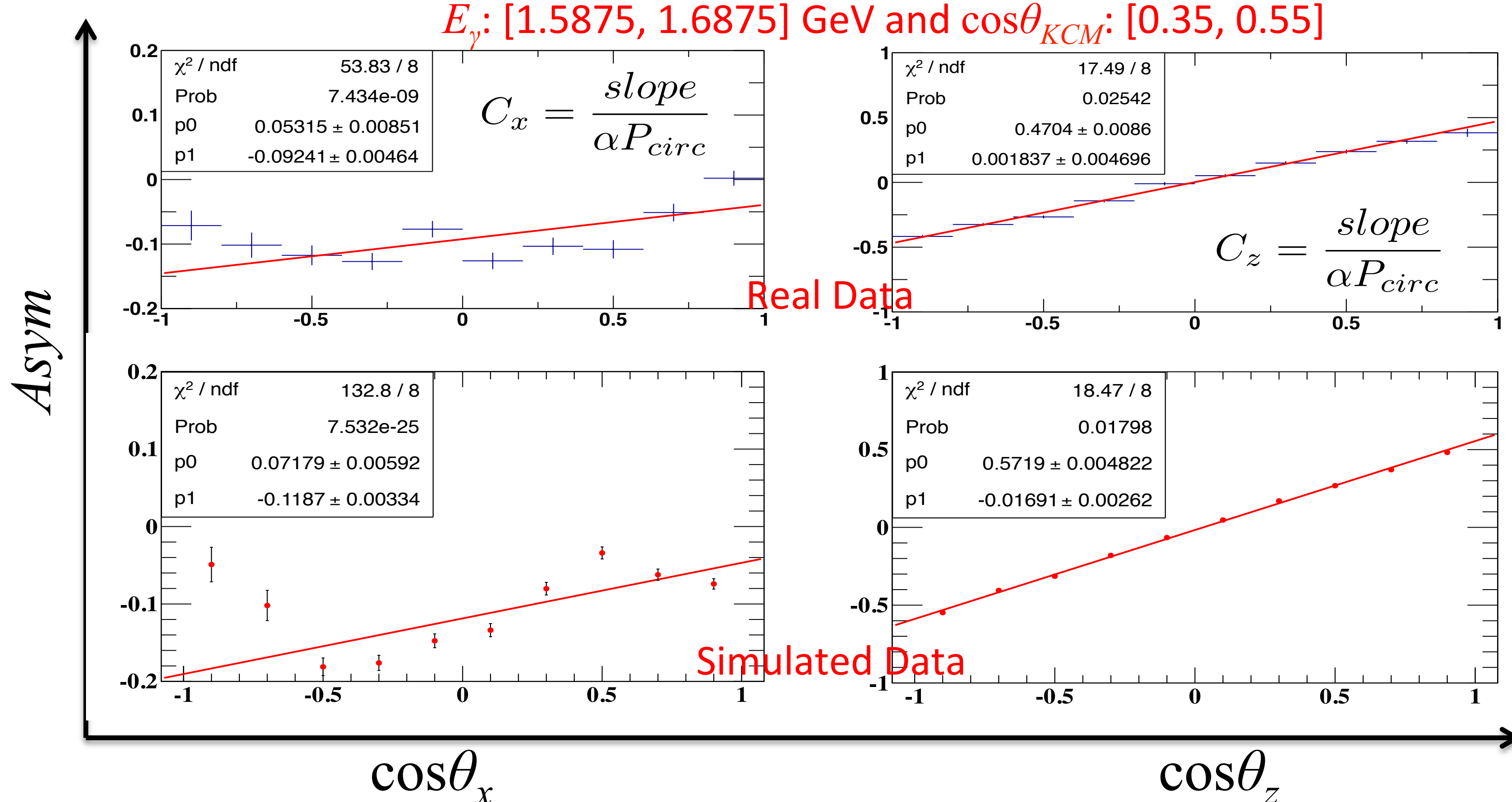

Statistical Uncertainties

A study by simulations is used to test if statistical uncertainties of the observables extracted by a computer program are reliable.

Function: σ vs. number of events

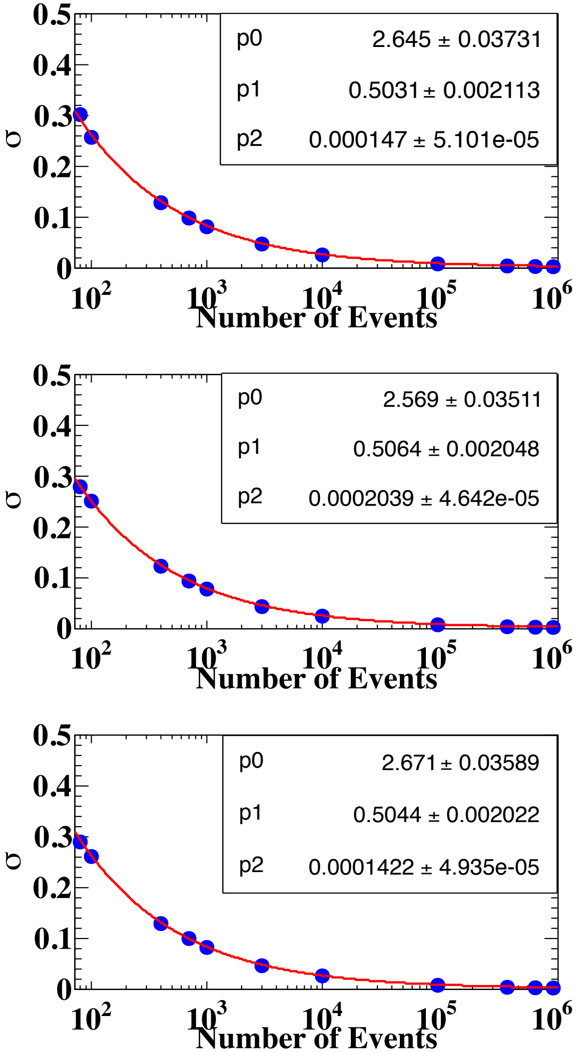

Difference between estimated and standard σ